

## TECHNICAL REPORT

Contract Title: Infrared Algorithm Development for Ocean Observations  
with EOS/MODIS  
Contract: NAS5-31361  
Type of Report: Semi-Annual  
Time Period: January- June 2000  
Principal Investigator: Otis B. Brown  
RSMAS/MPO  
University of Miami  
4600 Rickenbacker Causeway  
Miami, Florida 33149-1098

---

### INFRARED ALGORITHM DEVELOPMENT FOR OCEAN OBSERVATIONS WITH EOS/MODIS

#### Abstract

Efforts continue under this contract to develop and validate algorithms for the computation of sea surface temperature (SST) from MODIS infrared measurements. These include radiative transfer modeling, comparison of *in situ* and satellite observations, evaluation of surface validation approaches for IR radiances, and participation in MODIS (project) related activities. Of particular relevance in this reporting period is the first analysis of on-orbit data from MODIS on Terra.

#### A. NEAR TERM OBJECTIVES

##### MODIS Infrared Algorithm Development and Maintenance

- A.1. Algorithmic development efforts based on experimental match-up databases and radiative transfer models and inter-satellite comparisons
- A.2. Interaction with the MODIS Instrument Team through meetings and electronic communications, and provide support for MCST activities. Focus has been on analysis of the on-orbit data to determine the effects of instrumental artifacts.
- A.3. Maintain and develop at-sea instrumentation for MODIS SST validation.
- A.4. *In situ* validation cruises for the MODIS IR bands.
- A.5. Development and population of the M-AERI Data Base, the Oceanographic and Atmospheric Archive and Retrieval System (OAARS).

##### MODIS SST – Scientific Research

- A.6. Study thermal structure of ocean-atmosphere interface.
- A.7. Development of optimal skin-SST validation strategy.

##### Overarching Contract Activities

- A.8. Provide investigator and staff support for the preceding items.

## B. OVERVIEW OF CURRENT PROGRESS

January – June 2000

Activities during the past six months have continued on the previously initiated tasks. There have been specific efforts in the areas of analysis of on-orbit brightness temperatures and cruises to acquire MODIS infrared validation data. In addition, previously initiated activities, such as team related activities, continue, as have episodic efforts associated with MODIS anomaly characterization and response.

Special foci during this six-month period have been:

- 1) Refinement of the SST retrieval algorithm based on radiative transfer simulations of MODIS measurements.
- 2) With R. Evans, work on corrections for the instrumental artifacts in the MODIS SST bands.
- 3) Continuation of the analysis of measurements from M-AERI research cruises (Table 1).
- 4) Completion of the East Atlantic Transect on the *PFS Polarstern*
- 5) Preparation and participation in the cruise of the *USCGC Polar Star* from Australia to Seattle (March to May 2000).
- 6) Preparation and participation in the cruise of the Italian ship *R/V Urania* the Mediterranean Sea (March - April 2000).
- 7) Maintenance of the at-sea hardware.
- 8) Continue development of a purpose-built computer database for validation cruise data and associated satellite measurements.
- 9) Implementation of various SST data assimilation approaches.
- 10) In collaboration with Dr B. Ward of the Geophysical Institute, University of Bergen, Norway, on the analysis of subsurface temperature profiles from the autonomous SkinDeEP microstructure buoy.

### B.1. Algorithmic development efforts based on experimental match-up databases and radiative transfer models and inter-satellite comparisons.

The focus of the radiative transfer modeling and algorithm development has moved to the three SST bands in mid-infrared atmospheric window between 3.5 and 4.1 $\mu$ m wavelength (MODIS bands 20, 22,23). These have relatively invariable atmospheric transmission and offer the prospect of more accurate SST retrievals than possible in the conventional, thermal infrared window at 10-13 $\mu$ m wavelength (MODIS bands 31,32). However, because of sensitivity to sun-glint reflected at the ocean surface, retrievals of SST from these bands will be limited during the daytime.

## B.2. Interaction with the MODIS Instrument Team and support for MCST activities.

The arrival of the first data from MODIS was a welcome and long-awaited event, and the initial reaction was very positive. However, closer examination of the data revealed many of the anticipated instrumental artifacts, and others that came as a surprise. Those that were anticipated include detector banding, mirror side effects, and mirror reflectivity vs. scan angle; and those that were unanticipated include the extended dynamic range of bands 31 and 32, and noise in the least-significant-bit of the digital data. The extended dynamic range of bands 31 and 32 means that the advantage of 12-bit digitization over the 10-bits of AVHRR is lost and the radiometric resolution imposed by the digitizers

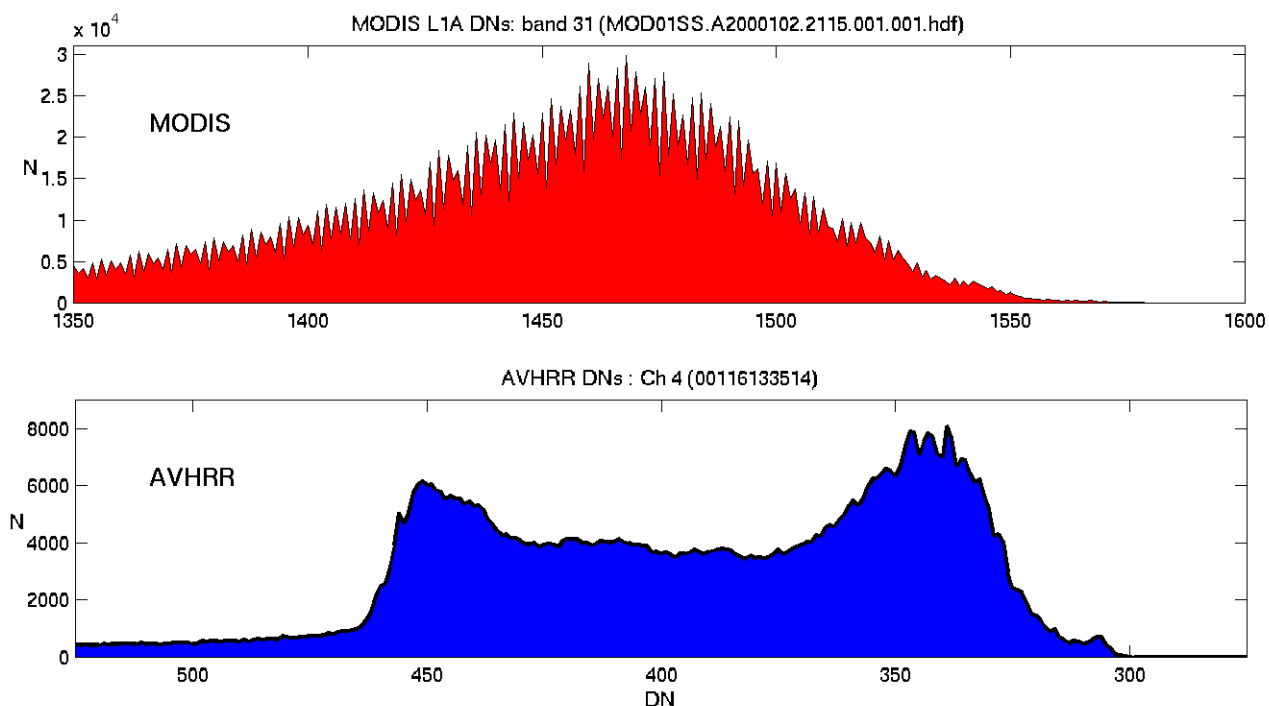


Figure 1. Histograms of digital counts from the  $\sim 11\mu\text{m}$  bands of MODIS and AVHRR over the ocean. The range of values, of about 200 counts is comparable, but the MODIS histogram shows a regular pattern indicative of digitizer errors. The AVHRR counts are plotted in decreasing values because of the inverse relationship with the measured radiances

is comparable for the two radiometers. Added to this the noise in the least-significant bit of MODIS means that the radiometric resolution of MODIS is poorer than AVHRR. Figure 1 shows examples of the histograms of digital counts from the  $\sim 11\mu\text{m}$  bands of MODIS and AVHRR over the ocean.

The results of the analysis of the digitizer errors were sent to Dr R. Murphy in a memorandum, which is attached to this report.

There have been interactions with Bob Evans (Contract NAS5-31362) and others at RSMAS on a daily basis to work on the characterization of MODIS instrumental issues; numerous telephone

discussion with Wayne Esaias, MODIS Oceans Team Leader on these problems and frequent exchanges of information and results with MCST members and with Raytheon personnel.

Wayne Esaias gave an invited presentation at the Spring Meeting of the AGU on early oceanographic results of the MODIS, and Eddie Kearns, of RSMAS, gave an invited seminar at the NOAA Atlantic Oceanographic and Atmospheric Laboratory on a similar topic. Peter Minnett made a presentation to the MODIS Science Team on the issues of deriving SST from MODIS measurements, and, earlier in the year, presented two posters at the DOE ARM (Atmospheric Radiation Measurements program) Science Team Meeting on the results of studies of accuracies of satellite measurements of SST and M-AERI measurements of air-sea temperature differences. At the “Gas Transfer at Water Surfaces Symposium,” held at Miami Beach, June 5-8, Jennifer Hanafin and Brian Ward presented posters on measurements of near-surface temperature structure, and the consequences of these on satellite-derived SST fields and on air-sea fluxes.

### B.3 Maintain and develop at-sea instrumentation for MODIS SST validation.

A new, stainless-steel enclosure for MAERI-1 was delivered and the instrument rebuilt into it. This is intended to provide a more secure environment for the interferometer unit. It increases the weight and volume of the unit, but provides a weatherproof enclosure that is more robust than the current wooden and plastic enclosures. If at-sea deployments are successful, additional enclosures will be built for MAERI-2 and MAERI-3.

The external weather-proof, air-conditioned and heated enclosed rack that encloses the M-AERI electronics and computer rack was deployed on the *Polar Sea* cruise from Australia to Seattle (see B.4). The new configuration will require the use of the thin, armored CAT-5 twisted pair cable to link the electronics unit to the real-time display in the lab. This is much more convenient and robust to deploy on the Coast Guard Ships that do not have convenient cable-ways and bulkhead feed-throughs. This is shown in Figure 2.

In collaboration with Dr R.M. Reynolds of the Brookhaven National Laboratory, a Portable Radiation Platform (PRP), comprising a Fast Rotating Shadowband Radiometer and broadband  $2\pi$  long- and short-wave radiometers, has been developed for installation with the M-AERIs and was used on the *Polar Sea* cruise from Australia to Seattle (see B.4) - Figure 3. The purpose of this is to determine the atmospheric aerosol parameters during MODIS overpasses.

### B.4 *In situ* validation cruises for the MODIS IR bands.

MAERI-3 completed the East Atlantic transect on the German ice-breaking research vessel *Polarstern* on its passage from Bremerhaven to Cape Town (section marked EAT in Figure 4). The instrument performed well, but storms in the winter north Atlantic, with high winds and extensive cloud cover, restricted the amount of useful data taken north of the tropics.

MAERI-2 was installed on the *USCGC Polar Star* in Melbourne, Australia, for the return section across the Pacific Ocean. The track is shown in Figure 4. Again, the instruments functioned well, and a wide range of environmental conditions were experienced during the cruise.

MAERI-3 was embarked on the Italian research vessel *Urania* in the western Mediterranean Sea. Compared to the other two deployments in this period, this one was focused on a small area of study in the Gulf of Lions between the Balearic Islands, Corsica and the northern Mediterranean coast. The track is shown in Figure 4. Again, the instruments functioned well.

The *Polar Star* and *Urania* cruises were the first to take place after MODIS on Terra began producing data and will provide the first validation data for the MODIS SSTs.



Figure 2. Deployment of the M-AERI on the USCGC *Polar Star* in March 2000. The M-AERI interferometer unit is under the silver-colored tarpaulin, with the scene mirror in the white enclosure to the left. The air-conditioned electronics and computer enclosure is the gray box a lower left. The small blue unit left of center is the DAR011 radiometer of Dr. Ian Barton of the CSIRO Marine Laboratory in Hobart, Australia.



Figure 3. The Portable Radiation Package installed on the USCGC *Polar Star* in March 2000. The sea-going Multifrequency Rotating Shadow band Radiometer (MFRSR) is the cylinder on the left, and the Eppley short-wave and long-wave  $2\pi$  radiometers are on the right. The box below contains the control computer, and the one below a back-up battery and power supply.

#### B.5 Development and population of the M-AERI Data Base, the Oceanographic and Atmospheric Archive and Retrieval System (OAARS).

The OAARS database is located at <http://www.rsmas.miami.edu/ir/maeri-db> and is constantly being populated with new data sets. Table 1 shows the current status of the database including number of records for each data type and cruise.

There are 15 completed M-AERI cruises detailed in Table 2. The time-line and cruise tracks of the completed projects are shown in Figure 4. The next step will be to add quality control flags to the data sets and further enhance the searching capabilities.

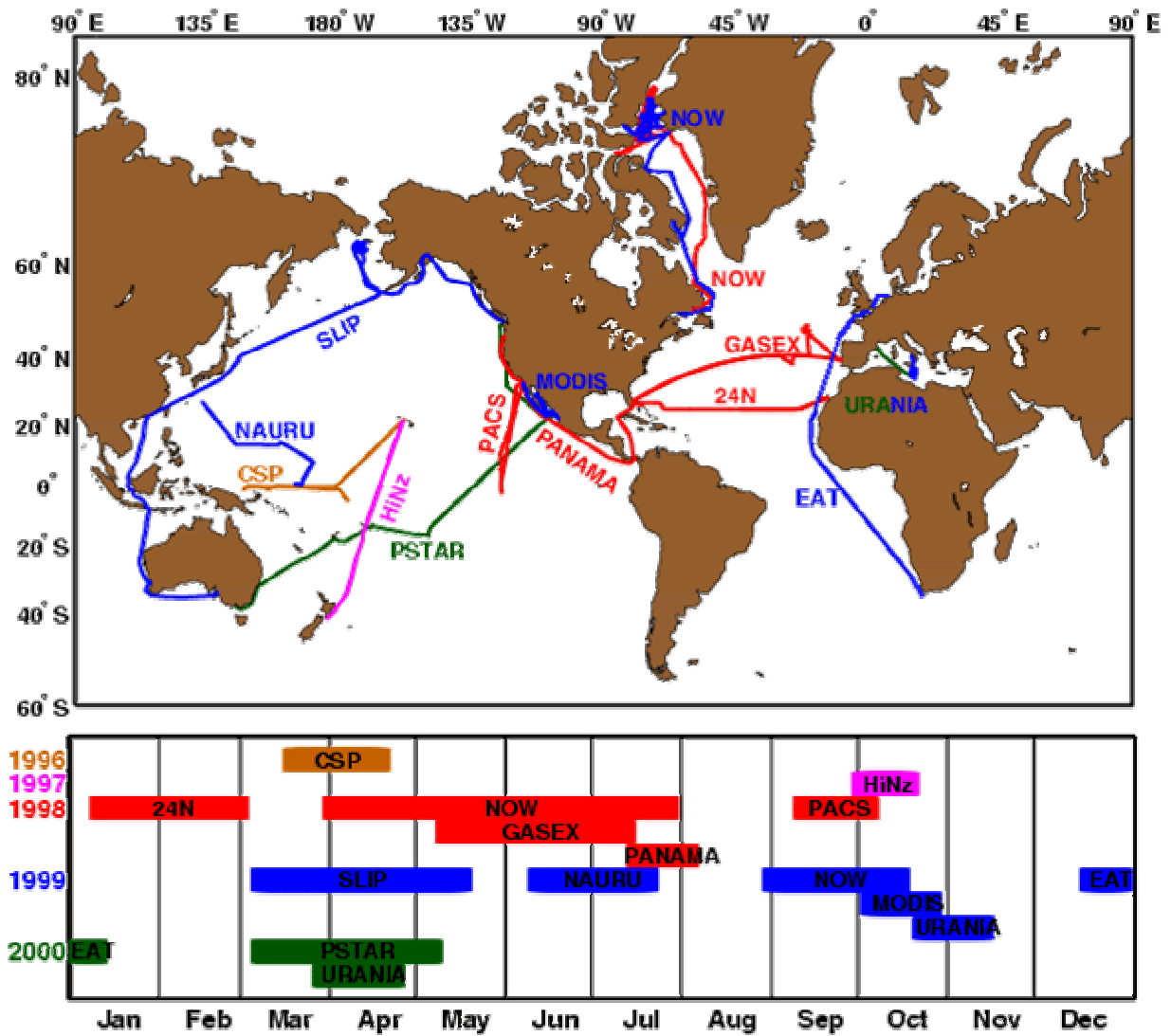


Figure 4. Chart and timeline of M-AERI cruises.

<b>Cruise</b>	<b>CSP</b>	<b>HiNz</b>	<b>24N</b>	<b>NOW</b>	<b>GASEX</b>	<b>PANAMA</b>	<b>PACS</b>	<b>SLIP</b>
<b>Year</b>	<b>1996</b>	<b>1997</b>	<b>1998</b>	<b>1998</b>	<b>1998</b>	<b>1998</b>	<b>1998</b>	<b>1999</b>
<b>DataName</b>								
MaeriSst	1429	2294	3090	23272	6773	2062	2904	6507
MaeriRet	19260							
MaeriQc			199	19565		12		53200
MaeriRad	See below	See below						
Ch1	25722560	19644345						
Ch2	25117440	18734268						
Stats	1101009	710304						
Wpac	Not Used	28915	65458	144008			Not Used	98316
ShipMet	84690		107483	Not Used	77505			
Tsg	78039	21600	107483	62273	83962	39955		
Rsonde	81594	1086	9593	208745	314969		207887	147535
HardHat	44085	Not Used		37441	66755	Not Used	2582	12673
ShipNav	255321		107483	876659				
Irt	51941	92676			Not Used			
ShipRad				5670				
Prp	Not Used	Not Used	Not Used					
Ctd			575407					
Xbt								
Adep			53519					
Org								

<b>Cruise</b>	<b>NAURU</b>	<b>NOW</b>	<b>MODIS</b>	<b>URANIA</b>	<b>EAT</b>	<b>PSTAR</b>	<b>URANIA</b>	<b>Total</b>
<b>Year</b>	<b>1999</b>	<b>1999</b>	<b>1999</b>	<b>1999</b>	<b>1999</b>	<b>2000</b>	<b>2000</b>	<b>Records</b>
<b>DataName</b>								
MaeriSst	2250	4874	2265	1658	2138	7102	2104	70722
MaeriRet								19260
MaeriQc								72976
MaeriRad								
Ch1								45366905
Ch2								43851708
Stats								1811313
Wpac				46855	32095	79626	30929	526202
ShipMet	25245		29195	12060	19455			355633
Tsg			29197	12060	21609	218213		674391
Rsonde			Not Used		10329	49020	25679	1056437
HardHat			37003	53584	Not Used	Not Used		254123
ShipNav	25245		29197	12062	17062	22202		1345231
Irt	Not Used		Not Used	Not Used	Not Used	Not Used	Not Used	144617
ShipRad	10602		29197					45469
Prp	22853			Not Used			Not Used	22853
Ctd				186224				761631
Xbt				7978				7978
Adep								53519
Org					12287			12287

Table 1. Current Data on OAARS

<b>Project</b>	<b>Ship</b>	<b>YYYYMMDD</b>	<b>Start Port</b>	<b>End Port</b>	<b>Instrument</b>
<b>CSP1996</b> Combined Sensor Cruise	NOAA Ship Discoverer	19960314-19960413	Pago-Pago, Am. Samoa	Honolulu, HI	Prototype
<b>HiNz1997</b> Hawaii-New Zealand Transit	R/V Roger Revelle	19970928-19971014	Honolulu, HI	Lyttleton, NZ	M-AERI 1 and 2
<b>24N1998</b> OACES 24 N Section	NOAA S Ronald H. Brown	19980108-19980224	Miami, FL	Miami, FL	M-AERI 1
<b>NOW1998</b> North Water	CCGS Pierre Radisson	19980316-19980728	Quebec City, Canada	Nanisivic, Canada	M-AERI 2
<b>GASEX1998</b> OACES Gasex	NOAA S Ronald H. Brown	19980502-19980707	Miami, FL	Miami, FL	M-AERI 1
<b>PANAMA1998</b> Panama Transit	NOAA S Ronald H. Brown	19980712-19980727	Miami, FL	Newport, OR	M-AERI 1
<b>PACS1998</b> PanAmerican Climate Studies-mooring recovery	R/V Melville	19980908-19980929	San Diego, CA	San Diego, CA	M-AERI 1
<b>SLIP1999</b> Western Pacific Transect, St. Lawrence Island Polynya	USCGS Polar Sea	19990301-19990511	Adelaide, Australia	Seattle, Washington	M-AERI 2
<b>NAURU1999</b>	R/V Mirai	19990608-19990720	Yokohama, Japan	Sikenehama, Japan	M-AERI 1
<b>NOW1999</b> North Water	CCGS Pierre Radisson	19990824-19991010	Quebec City, Canada	Quebec City, Canada	M-AERI 2
<b>MODIS1999</b>	R/V Melville	19991001-19991020	San Diego, CA	San Diego, CA	M-AERI 1
<b>URANIA1999</b>	NAVE Urania	19991019-19991109	Messina, Sicily	Civitavechhia, Italy	M-AERI 3
<b>EAT1999</b> Eastern Atlantic Transect	R/V Polarstern	19991215-20000106	Bermerhaven, Germany	Cape Town Africa	M-AERI 3
<b>PSTAR2000</b> Pacific Transect	USCGC Polar Star	20000304-20000501	Melbourne, Australia	Seattle, WA	M-AERI 2
<b>URANIA2000</b> Gulf of Lions	R/V Urania	20000325-20000418	Naples, Italy	Naples, Italy	M-AERI 3

Table 2 Completed M-AERI Cruises

## MODIS SST – Scientific Research

### B.6 Study thermal structure of ocean-atmosphere interface.

Analysis of the M-AERI data taken during the cruise of the R/V Melville in the Pacific Ocean and Gulf of California in October 1999 is revealing some of the complexity of the effects of the thermal skin layer and the diurnal thermocline. A wide range of surface temperatures and wind speeds were encountered during this cruise, but the behavior of the skin temperature, when referenced to the bulk temperature measured by the ship's thermosalinograph at a depth of ~3m shows consistency. Figure 5 shows the time series of bulk temperature (black line in the top panel) and skin temperature (line in top panel colored by local sun time) for the duration of the cruise. The center panel shows the skin-bulk temperature difference, again colored by local sun time, and the lower panel the surface wind speed, corrected for the ship's motion. During the night, and for conditions of moderate wind speed the skin is consistently cooler than the underlying bulk temperatures, by up to several tenths of a degree. For conditions of low wind speed during the day, the heat absorbed in the uppermost several meters of the water column is not mixed and gradients can build up over the course of the day. This is very apparent when the skin-bulk temperature difference is plotted as a function of local sun time and colored by local wind (Figure 6). At low wind speeds, under the conditions experienced during this cruise, diurnal decoupling of the skin layer from the bulk temperature at 3 m can be as large as 4K. This is a very significant in terms of validating satellite-derived SSTs at the level of a few tenths of a degree. As the wind speed increases, the amplitude of the diurnal signal decreases and the time of maximum skin temperatures moves to later in the afternoon. Plotting the same data as a function of wind speed (Figure 7) shows how the skin-bulk difference collapses to a much less variable distribution at winds of  $6\text{ms}^{-1}$  and more. This implies that there may be a role for bulk temperature measurements in the validation of MODIS SSTs if these are taken at night or on windy days, provided the small but significant wind-speed dependent offset is taken into account.

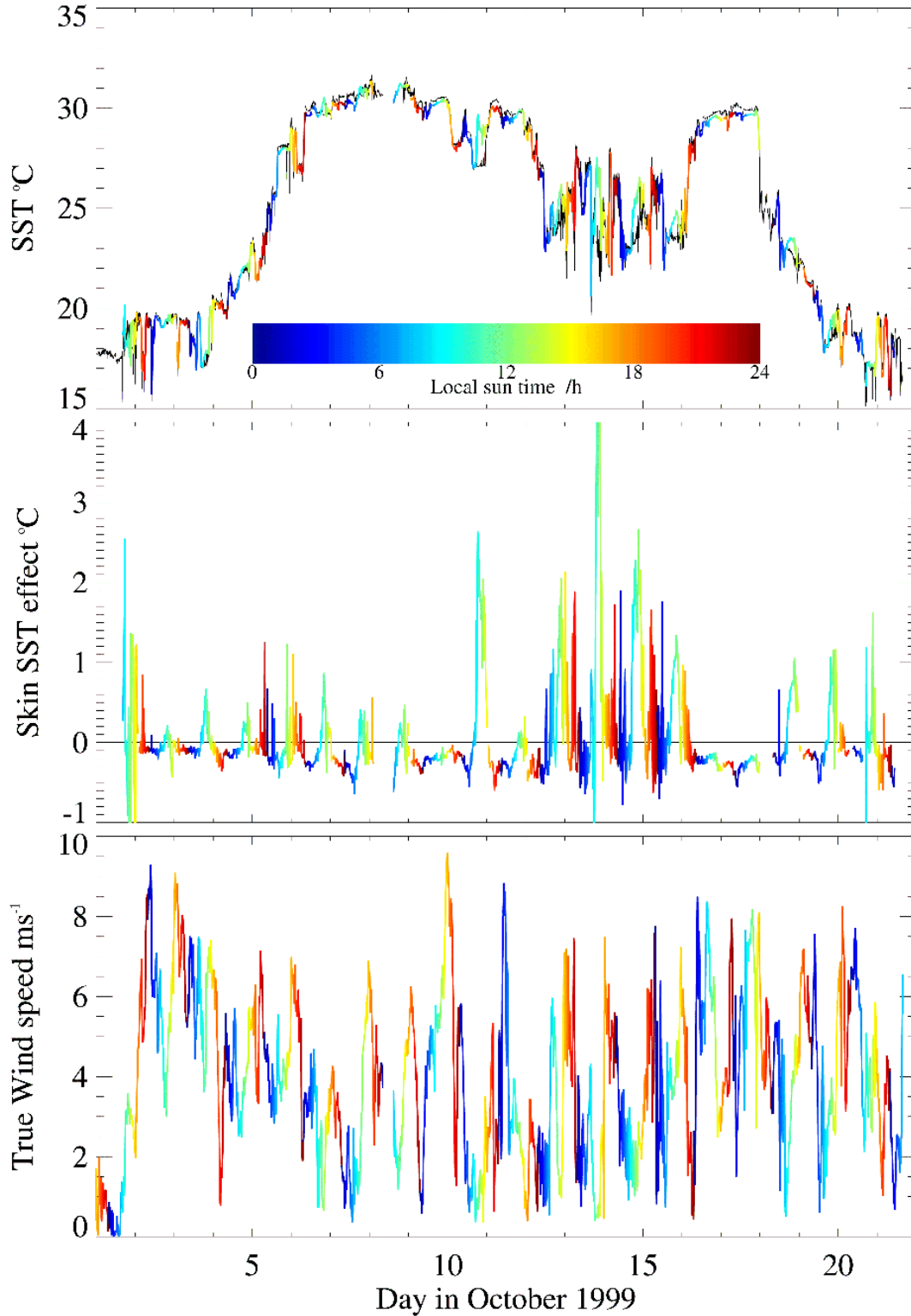


Figure 5. Time series of measurements taken during the MOCE-5 cruise of the R/V *Melville*, 1-21 October, 1999. The top panel shows bulk (3m depth) SST (black) and skin temperature measured by the M-AERI colored by local sun time, and the center panel the difference between these. The bottom panel shows the wind speed, corrected for the effects of ship motion.

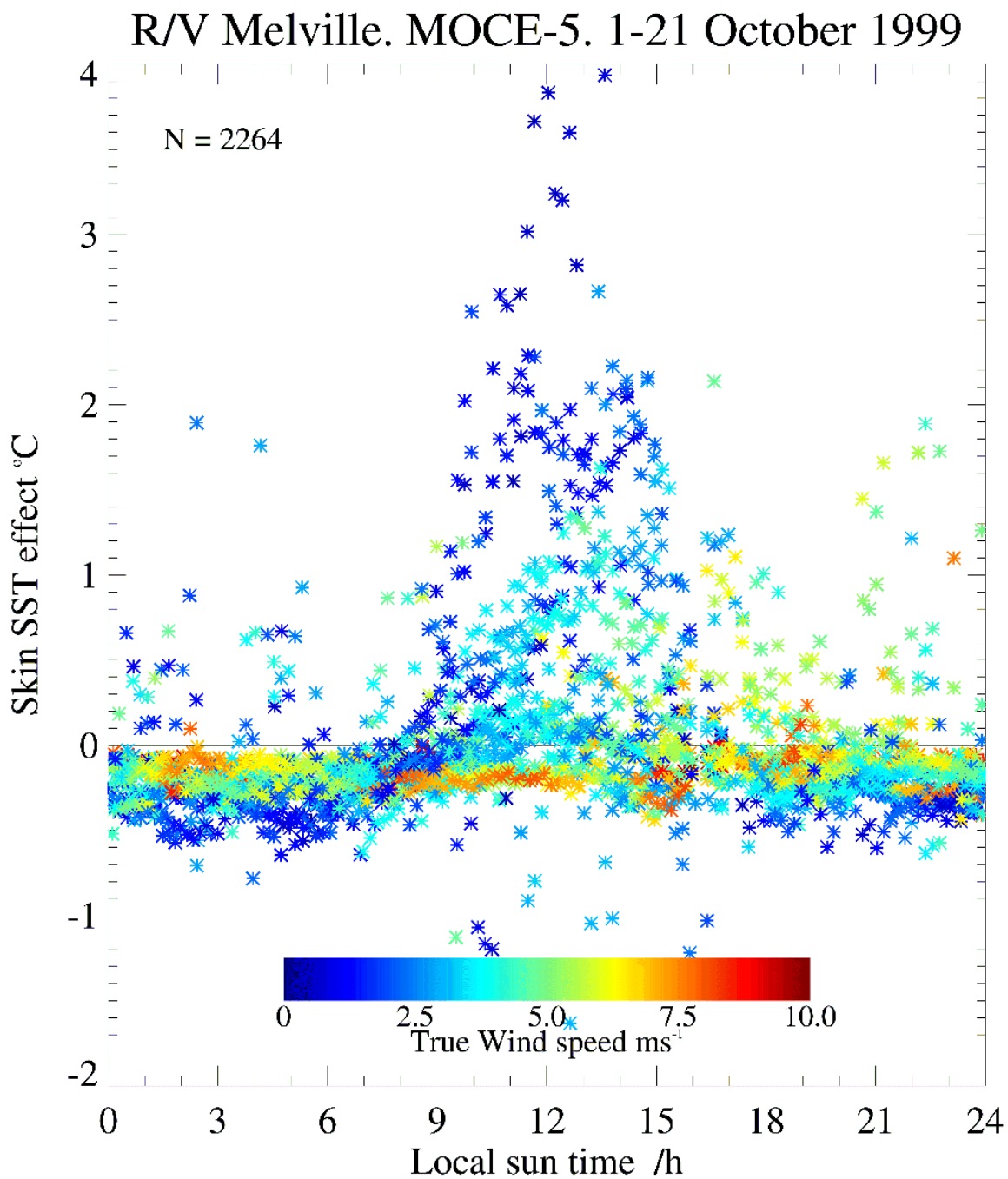


Figure 6. Measurements of the skin-bulk temperature difference taken during the MOCE-5 cruise of the R/V Melville, 1-21 October 1999, colored by wind speed, corrected for the effects of ship motion.

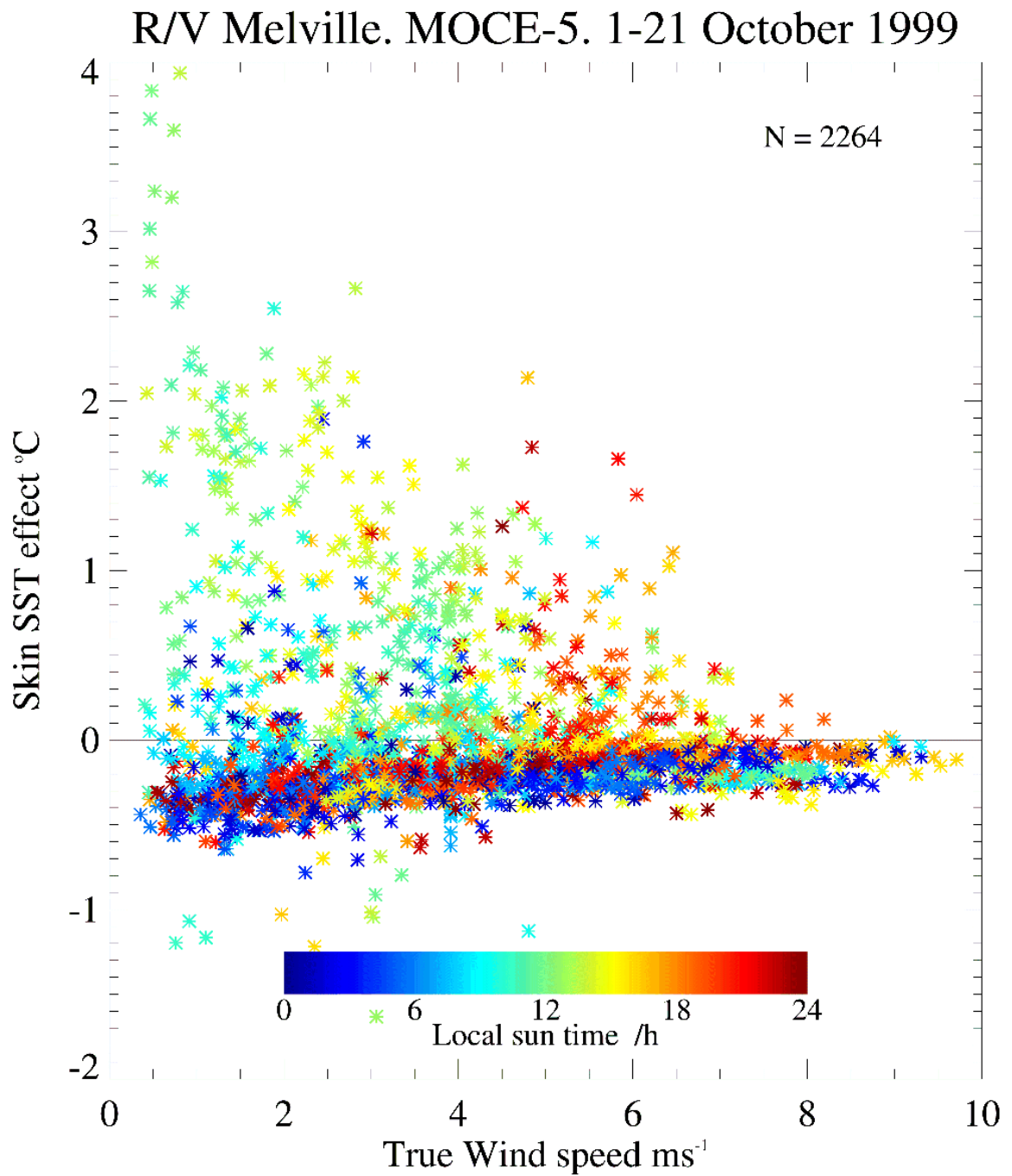


Figure 7. Measurements of the skin-bulk temperature difference taken during the MOCE-5 cruise of the R/V Melville, 1-21 October, 1999, colored by local sun time.

### C. Investigator Support

<b>January</b>	W. Baringer O. Brown M. Framinan K. Kilpatrick	R. Kolaczynski R. Kovach K. Maillet A. Mariano	J. Splain M. Szczodrak S. Walsh
<b>February</b>	W. Baringer J. Brown O. Brown M. Framinan K. Kilpatrick	R. Kolaczynski R. Kovach A. Li K. Maillet	A. Mariano J. Splain M. Szczodrak S. Walsh
<b>March</b>	W. Baringer J. Brown O. Brown M. Framinan K. Kilpatrick R. Kolaczynski	R. Kovach A. Li R. Jones K. Maillet A. Mariano	P. Minnett R. Sikorski J. Splain M. Szczodrak S. Walsh
<b>April</b>	W. Baringer J. Brown O. Brown M. Framinan K. Kilpatrick	R. Kolaczynski R. Kovach J. Hargrove K. Maillet A. Mariano	P. Minnett R. Sikorski J. Splain M. Szczodrak S. Walsh
<b>May</b>	W. Baringer J. Brown O. Brown M. Framinan K. Kilpatrick	R. Kolaczynski R. Kovach J. Hargrove A. Li	K. Maillet A. Mariano M. Szczodrak S. Walsh
<b>June</b>	W. Baringer J. Brown M. Framinan K. Kilpatrick R. Kolaczynski	R. Kovach A. Li K. Maillet A. Mariano	R. Sikorski J. Splain M. Szczodrak S. Walsh

## **D. Future Activities**

### **D.1 Algorithms**

- a. Continue to develop and test algorithms on global retrievals
- b. Evaluation of global data assimilation statistics for SST fields
- c. Participate in research cruises
- d. Continue radiative transfer modeling
- e. Continue analysis of research cruise data
- f. Continue to study near-surface temperature gradients
- g. Continue planning of post-launch validation campaigns
- h. Validation Plan updates (as needed)
- i. EOS Science Plan updates (as needed)
- j. Continued participation in MODIS Team activities

### **D.2 Investigator support**

Continue appropriate efforts.

### **D.3 Presentations and publications.**

- a. Prepare material for the *Gas Transfer at Water Surfaces* Symposium in Miami Beach, the Oceans from Space 2000 Symposium in Venice, the ESA Envisat Symposium in Gothenberg, and the PORSEC 2000 Symposium in Goa.
- b. Prepare scientific results for publication in the refereed literature.

## **E. Problems**

The instrumental artifacts in the SST bands evident in the on-orbit data from MODIS are very disconcerting. They are more severe than anticipated and their consequences on the absolute accuracy of the SSTs are likely to result in the performance of MODIS not matching that of AVHRR. It is imperative that the appropriate steps be taken to correct these in the FM-1 MODIS before launch.

## **F. Publications and Presentations**

### F.1 Refereed publications:

Hanafin, J. A. and P. J. Minnett, 2001. Profiling temperature in the sea surface skin layer using FTIR measurements. *Gas Transfer at Water Surfaces*. edited by M. A. Donelan, W.M. Drennan, E.S. Saltzmann and R. Wanninkhof. *American Geophysical Union Monograph*. Submitted.

*Sea surface spectral emissivity and the depth of the thermal skin boundary layer were determined using high spectral resolution measurements of the sea surface and the atmosphere taken in the field measurements by the Marine-Atmosphere Emitted Radiance Interferometer. In order to determine the sea surface emissivity, the effective incidence angle was found by minimizing the variance in the brightness temperature spectrum retrieved from the corrected upwelling radiance spectrum. Certain wavelength regions have different absorption characteristics, allowing the temperature at different levels to be retrieved from different spectral regions. In this way, the temperature gradient of the*

*thermal boundary layer was determined. The depth of the skin layer was then calculated by determining the depth at which the thermometrically measured bulk temperature intersects this gradient. At low wind speeds, the skin layer can be up to 0.2mm deep, getting shallower with increased wind speed and becoming very shallow (0.01-0.07mm) above wind speeds of  $8\text{ms}^{-1}$ . These results are encouraging for application of this method to determine air-sea heat and gas fluxes in the field.*

Kearns, E.J., J.A. Hanafin, R.H. Evans, P.J. Minnett and O.B. Brown, 2000. An independent assessment of Pathfinder AVHRR sea surface temperature accuracy using the Marine-Atmosphere Emitted Radiance Interferometer (M-AERI). *Bull. Am. Met. Soc.* Accepted.

*The remotely sensed sea surface temperature (SST) estimated from the 4-km-resolution Pathfinder SST algorithm is compared to a SST locally measured by the Marine Atmospheric Emitted Radiance Interferometer (MAERI) during five oceanographic cruises in the Atlantic and Pacific Oceans, in conditions ranging from Arctic to equatorial. The Pathfinder SST is a product of the satellite-based Advanced Very High Resolution Radiometer, while the MAERI is an infrared radiometric interferometer with continuous onboard calibration that can provide highly accurate (better than  $0.05^{\circ}\text{C}$ ) in situ skin temperatures during extended shipboard deployments. Matchups, which are collocated (within 4 km) and coincident ( $\pm 40$  min during the day;  $\pm 120$  min during the night) data, from these two different sources under cloud-free conditions are compared. The average difference between the MAERI and Pathfinder SSTs is found to be  $0.07 \pm 0.31^{\circ}\text{C}$  from 219 matchups during the low- and mid-latitude cruises; inclusion of 80 more matchups from the Arctic comparisons produces an average global difference of  $0.14 \pm 0.36^{\circ}\text{C}$ . The MAERI-Pathfinder differences compare favorably with the average mid-latitude differences between the MAERI skin SST and other bulk SST estimates commonly available for these cruises such as the research vessels' thermosalinograph SST ( $0.12 \pm 0.17^{\circ}\text{C}$ ) and the weekly National Centers for Environmental Prediction optimally interpolated SST analysis ( $0.41 \pm 0.58^{\circ}\text{C}$ ). While not representative of all possible oceanic and atmospheric regimes, the accuracy of the Pathfinder SST estimates under the conditions sampled by the five cruises is found to be at least twice as good as previously demonstrated.*

Kumar, A., P. J. Minnett, G. Podesta, and R.H. Evans, 2000. Analysis of Pathfinder SST algorithm for global and regional conditions. Special Issue on the International JGOFS Symposium on 'Biogeochemistry of the Arabian Sea' *Proceedings of the Indian Academy of Sciences: Earth and Planetary Sciences*, Accepted

*As part of the Pathfinder program developed jointly by National Aeronautics and Space Administration (NASA) and National Oceanic and Atmospheric Administration (NOAA) a large database of in situ sea surface temperature (SST) measurements coincident with satellite data is now available to the user community. The Pathfinder Matchup Database (PMDDB) is a multi-year, multi-satellite collection of coincident measurements from the Advanced Very High Resolution Radiometer (AVHRR) and broadly distributed buoy data (matchups). This database allows the user community to test and validate new SST algorithms to improve the present accuracy of surface temperature measurements from satellites. In this paper we investigate the performance of a global Pathfinder algorithm to specific regional conditions. It is shown that for zenith angles less than  $45^{\circ}$ , the best-expected statistical discrepancy between satellite and buoy data is about  $\sim 0.5\text{K}$ . In general, the bias of the residuals (satellite - buoy) is negative in most regions, except in the North Atlantic and adjacent seas, where the residuals are always positive. A seasonal signal in SST residuals is observed in all regions and is strongest in the Indian Ocean. The channel-difference term used as a proxy for atmospheric water vapor correction is observed to be unresponsive for columnar water vapor values greater than 45 mm and high zenith angles. This unresponsiveness of the channels leads to underestimation of sea surface temperature from satellites in these conditions.*

Minnett, P.J., 2001, Satellite Remote Sensing: Sea Surface Temperatures. *Encyclopedia of Ocean Sciences*, J. Steele, S. Thorpe, K. Turekian (eds). Academic Press, London, UK. Submitted.

*The ocean surface is the interface between the two dominant, fluid components of the earth's climate system: the oceans and atmosphere. The heat moved around the planet by the oceans and atmosphere helps make much of the earth's surface habitable, and the interactions between the two, that take place through the interface, are important in shaping the climate system. The exchange between the ocean and atmosphere of heat, moisture and gases (such as  $\text{CO}_2$ ) are*

determined, at least in part, by the sea surface temperature (SST). Unlike many other critical variables of the climate system, such as cloud cover, temperature is a well-defined physical variable that can be measured with relative ease. It can also be measured to useful accuracy by instruments on earth-observation satellites.

The major advantage of satellite remote sensing of SST is the high-resolution global coverage provided by a single sensor, or suite of sensors on similar satellites, that produces a consistent data set. By the use of on board calibration, the accuracy of the time series of measurements can be maintained over years, even decades, to provide data sets of relevance to research into the global climate system. The rapid processing of satellite data permits the use of the global-scale SST fields in applications where the immediacy of the data is of prime importance, such as weather forecasting, with the prediction of the intensification of tropical storms and hurricanes a particular example.

Minnett, P. J., R. O. Knuteson, F.A. Best, B.J. Osborne, J. A. Hanafin and O. B. Brown, 2001. The Marine-Atmosphere Emitted Radiance Interferometer (M-AERI), a high-accuracy, sea-going infrared spectroradiometer. *Journal of Atmospheric and Oceanic Technology*. In revision.

*The Marine-Atmospheric Emitted Radiance Interferometer (M-AERI) is described and some examples of the environmental variables that can be derived from its measurements, and the types of research that these can support are briefly presented. The M-AERI is a robust, accurate, self-calibrating, sea-going Fourier-transform interferometric infrared spectroradiometer that is deployed on marine platforms to measure the emission spectra from the sea surface and marine atmosphere. The instrument works continuously under computer control and functions well under a very wide range of environmental conditions with a high rate of data return. Spectral measurements are made in the range of ~3 to ~18  $\mu\text{m}$  wavelength, and are calibrated using two internal, NIST-traceable blackbody cavities. The environmental variables derived from the spectra include the surface skin temperature of the ocean, surface emissivity, near-surface air temperature and profiles of temperature and humidity through the lower troposphere. These measurements are sufficiently accurate both to validate satellite-derived surface temperature fields, and to study the physics of the skin layer.*

Ward, B. and P. J. Minnett, 2001. An autonomous profiler for near surface temperature measurements. *Gas Transfer at Water Surfaces*. edited by M. A. Donelan, W.M. Drennan, E.S. Saltzmann and R. Wanninkhof. *American Geophysical Union Monograph*. Submitted.

*This paper describes the profiling instrument SkinDeEP (Skin Depth Experimental Profiler), which measures the temperature of the water column from a depth of about 6 meters to the surface with high resolution thermometers. The instrument operates in an autonomous mode as it has the capability to change buoyancy by inflating a neoprene bladder attached to the body of the profiler. Measurements are recorded only during the ascending phase of the profile so as to minimize disturbances at the surface. Results from deployment of the profiler show strong temperature gradients within the bulk waters under conditions of high insolation. These data were compared to the skin temperatures as measured by the M-AERI, a high accuracy interferometric infrared spectroradiometer. The corresponding bulk-skin temperature differences ( $\Delta T$ ) were shown to have strong dependence on the depth of the bulk measurement during the daytime with low wind speeds, but at higher wind speeds, the depth dependence vanishes. One set of profiles under nighttime conditions is also presented, showing the presence of overturning and thus a heterogeneous temperature structure within the bulk.*

Yang, Q, Parvin, B, and Mariano, A. J., 2000. Detection of vortices and saddle points in SST data. *Geophysical Research Letters*, **28**, 331-334.

*We extend the Horn-Schunck model of flow field computation to incorporate incompressibility for tracking fluid motion. This is expressed as a weak form of zero-divergence constraint in the variational problem and implemented with a multigrid approach for efficient computation. The resulting feature displacement velocity field provides the basis for higher level abstraction and representation of the data for data mining. A robust and efficient algorithm, based on the Jordan curve index, for detecting vortices and saddle points in feature displacement fields derived from sequences of satellite-derived SST fields is presented.*

## F.2 Presentations:

Brown, O.B., P. J. Minnett, R. H. Evans, E. J. Kearns, and R. J. Sikorski. MODIS Sea-surface temperature. MODIS Science Team Meeting, College Park, MD. June 7-8, 2000.

Esaias, W., M. Abbott, J. Campbell, K. Carder, O. Brown, D. Clark, R. Evans, F. Hoge, H. Gordon, P. Minnett. Early MODIS Ocean Data Results. Spring Meeting of the American Geophysical Union. Washington, DC. May 30-June 3, 2000.

Hanafin, J.A. and P.J. Minnett, Profiling Temperature in the Sea Surface Skin Layer Using FTIR Measurements. Gas Transfer at Water Surfaces Symposium, Miami Beach, Florida, USA. June 5-8, 2000.

Kearns, E. J., R. H. Evans, P. J. Minnett, O. B. Brown, K. Kilpatrick, S. Walsh, W. Baringer, J. Brown, and R. Sikorski. New SST and Ocean Color Data from MODIS/Terra: Caveat Emptor? NOAA Atlantic Oceanographic and Meteorological Laboratory, Miami, FL, June 2, 2000.

Minnett, P.J., E. J. Kearns, J. A. Hanafin, R. H. Evans and O.B. Brown Improved determination of the accuracy of satellite-derived SST fields. Tenth ARM Science Team Meeting, San Antonio, TX, 13-17 March 2000.

Minnett, P.J. Modulation of the skin-bulk sea-surface temperatures measured from the R/V *Mirai* during Nauru99. Tenth ARM Science Team Meeting, San Antonio, TX, 13-17 March 2000.

Ward, B. and P.J. Minnett, An autonomous profiler for near surface temperature measurements. Gas Transfer at Water Surfaces Symposium, Miami Beach, Florida, USA. June 5-8, 2000.

## Appendix – Memorandum to Dr. R. Murphy on *Terra* MODIS Digitizer issues.

---

April 5, 2000

Dr R. Murphy  
GSFC

Re: Digitizer problems in the Terra MODIS bands used for the measurement of Sea-Surface Temperature.

Bob,

In response to your request for clarification on the A/D problems we are sending you some plots that show the statistics of the A/D characteristics, and indicate how they influence the measurements of SST. Attached are some plots of the distributions of digital values in a representative MODIS granule for bands 20, 22, 23, 31 and 32. Also attached are histograms of bit occupancy in the digital values from this granule. The data for these plots have been separated by detector.

We have analyzed instrument behavior by wave band for bands 20, 22, 23, 31 and 32 for all 10 detectors for each band. Histograms were constructed by counting the number of occurrences of each ADC count for each band and detector (figures 1, 2, 3, 4, 12, 13, 14 and 15). The count patterns showing excess/loss of counts is specific for the count, regardless of which band/detector is chosen. These patterns repeat for the short wave (bands 20,22,23) and long wave bands (31, 32) showing patterns that are specific by focal plane.

An additional problem is associated with the long wave bands. Figure 15 shows noise that is dependent on the detector where spikes in counts are repeated for a specific detector in both bands 31 and 32. The distribution of noise changes according to which detector is analyzed suggesting that the counts are contaminated by noise. Analysis of the histograms of bit frequency, figures 16, 17, 18, and 19, shows the distribution of bit frequency is strongly detector dependent for bands 31 and 32 where the corresponding bit frequency histograms for the short wave IR bands are approximately uniform for the low order bits (Figures 6 to 11).

If the ADC were working well we would expect the histograms of digital counts to be smooth and the occupancy levels of the lower order bits to be 50%. Neither is the case.

The histograms of digital counts from the single granule show:

- a) A distinct odd-even anomaly in all detectors, but showing detector dependency.
- b) The modulation of the histograms show features at intervals of 2, 4, 8, 16 indicating that the problem is not restricted to just the least significant bit, or if it predominantly an lsb feature, it acts to exert an influence on higher bits.
- c) Band groups (20, 22, 23) and (31, 32) show different characteristics - they have different ADC systems.

d) Within each set of bands the characteristics are more similar for the same detector number (channels) than for different detectors within each band. This is worrisome and unexpected: as we understand it, each set of detectors within a band share the same digitizer, which is different for each band. Thus this cannot simply be the result of rogue ADCs as this would lead to similarities within bands, not across detectors. Something appears to be injecting noise into the system in such a way it is in synchrony with detector read-out.

The histograms of bit occupancy show that, in general, all low order bits are below the expected 50% level. The problem is not simply a least significant bit issue (i.e., alternate bins being "narrow"), which would manifest itself with bit 0 showing low (or high) occupancy with all others showing 50%. (The 50% level is not anticipated for high order bits as the environmental signal is not expected to fill the dynamic range of each detector uniformly). These results indicate problems up to the 4th or 5th bit. This type of plot is a sensitive indicator of systematic problems with the ADCs, but this does not imply that the data can be corrected.

Another similar analysis used 15 different MODIS granules from day 92 to provide the scene variability to more completely sample the dynamic range. This allows enhanced statistical significance for the distributions of the 4th and 5th bits and permits a more quantitative analysis. Figures 9, 10, 11, 18 and 19 show the results of this analysis. The results from the multi-granule analysis support the conclusions drawn from the examination of the single granule -- mainly that there are indeed systematic problems with the ADCs that extend to or beyond the 4th bit.

It is clear that the ADCs are not functioning optimally, and it is also clear that their characteristics indicate that the problem is not simply noise at the least significant bit level. Given that redundancy is available for each component in the digitizer channels, cross-strapping experiments between pairs of components are needed to determine the optimum configuration to reduce these unwanted characteristics.

It is very difficult to quantify the consequences of this behavior on SST determination, as it is clearly not simply a case of noise being imposed on every pixel. It is clear, however, that some pixel values are being erroneously digitized, up to and including the 5th bit. Using the information provided by Jack Xiong (MCST) we note that the digitization increment at T=290K corresponds to the following brightness temperature differences of

Band	dT
20	0.033
22	0.026
23	0.026
31	0.057
32	0.055

The brightness temperature differences are, of course, increased by 2, 4, 8, 16, etc. for increasing bit number.

These values for bands 31 and 32 are comparable to those of the 10-bit digitized values from the corresponding channels of AVHRR. That means the potential advantage of the extra 2-bits of MODIS digitization is not being realized. This can be seen in the histograms of the digital values, which show most of the environmental signal being represented in a range of about 500 digital numbers out of a total range of 4096.

Note that the atmospheric correction algorithm magnifies the size of the brightness temperature uncertainties, generally by a factor of two to three, when SST is derived.

Examination of SST images derived from bands 31 and 32 of MODIS, in areas where the atmosphere appears to be clear and the SST to be relatively uniform, reveals the following characteristics:

- a) mirror-side-to-mirror-side banding of amplitude of about 1/4 degree
- b) detector-to-detector banding of amplitude of about 1/4 degree
- c) a grainy appearance, on scales of 10km and less, with an amplitude of about 3/4 degree.

By comparison, the corresponding SST image derived from band 22 and 23 do not show a), b) is dominated by the bad data from detector 4 in band 22. The level of graininess is below 1/4 degree.

These fields are derived with the best available 're-normalization' between detectors. The graininess can be presumed to be a consequence, at least in part, of the ADC problems.

Note, at this point we cannot make a statement of the absolute accuracy of the SST fields.

We hope this explains our concerns clearly. Further, we hope that the cross-strapping exercise will be carried out, and lead to better MODIS data.

Sincerely,

Dr. O. B. Brown  
Dr. R. H. Evans  
Dr. E. J. Kearns  
Dr. P. J. Minnett

The Rosenstiel School of Marine and Atmospheric Sciences  
Meteorology and Physical Oceanography Division  
University of Miami  
4600 Rickenbacker Causeway  
Miami, FL 33149-1098

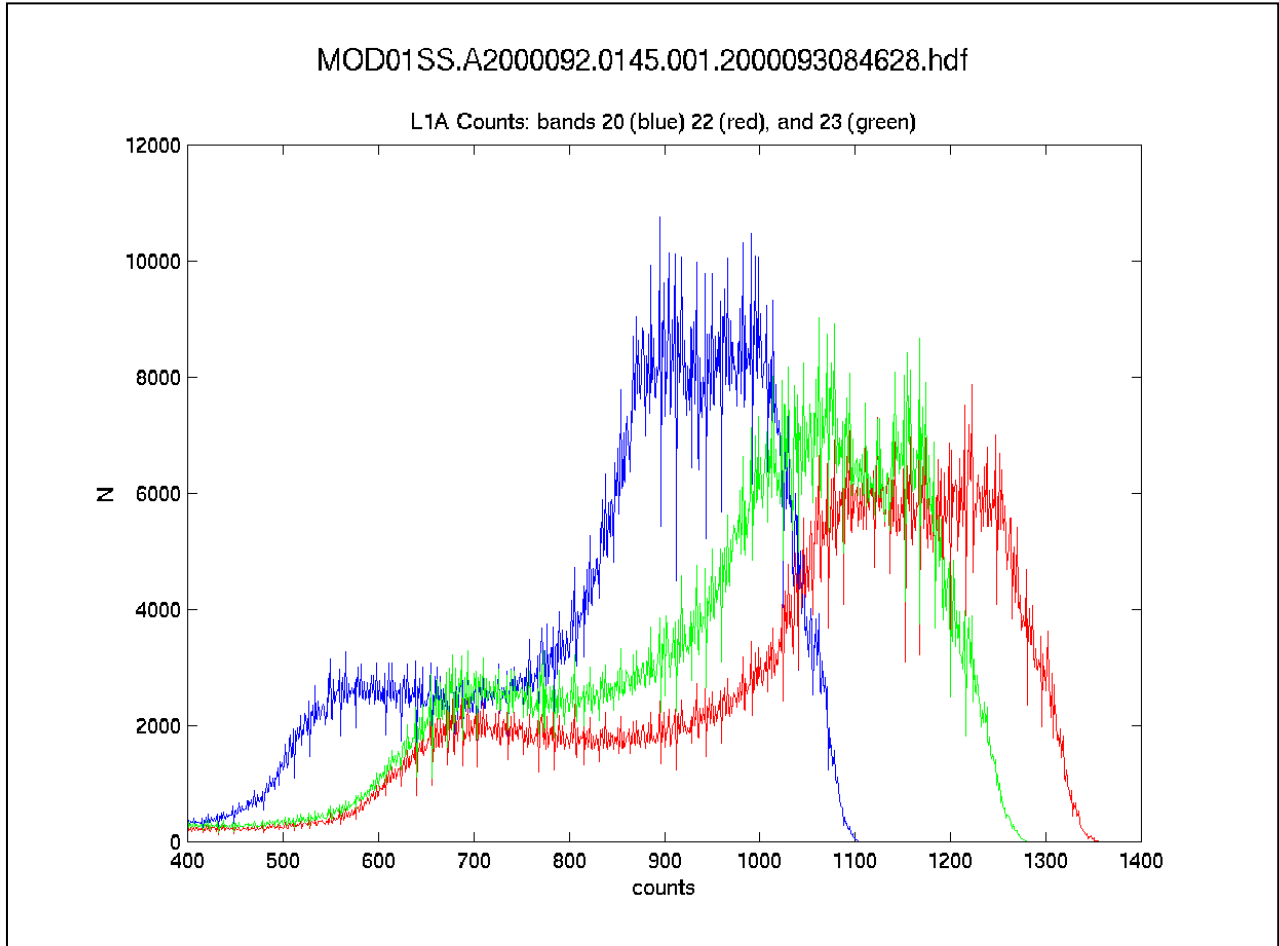


Figure 1. Histogram of the occurrence of digital counts in Bands 20, 22 and 23 at Level 1a processing for one granule. Output from all channels (detectors) are shown.

MOD01SS.A2000092.0145.001.2000093084628.hdf

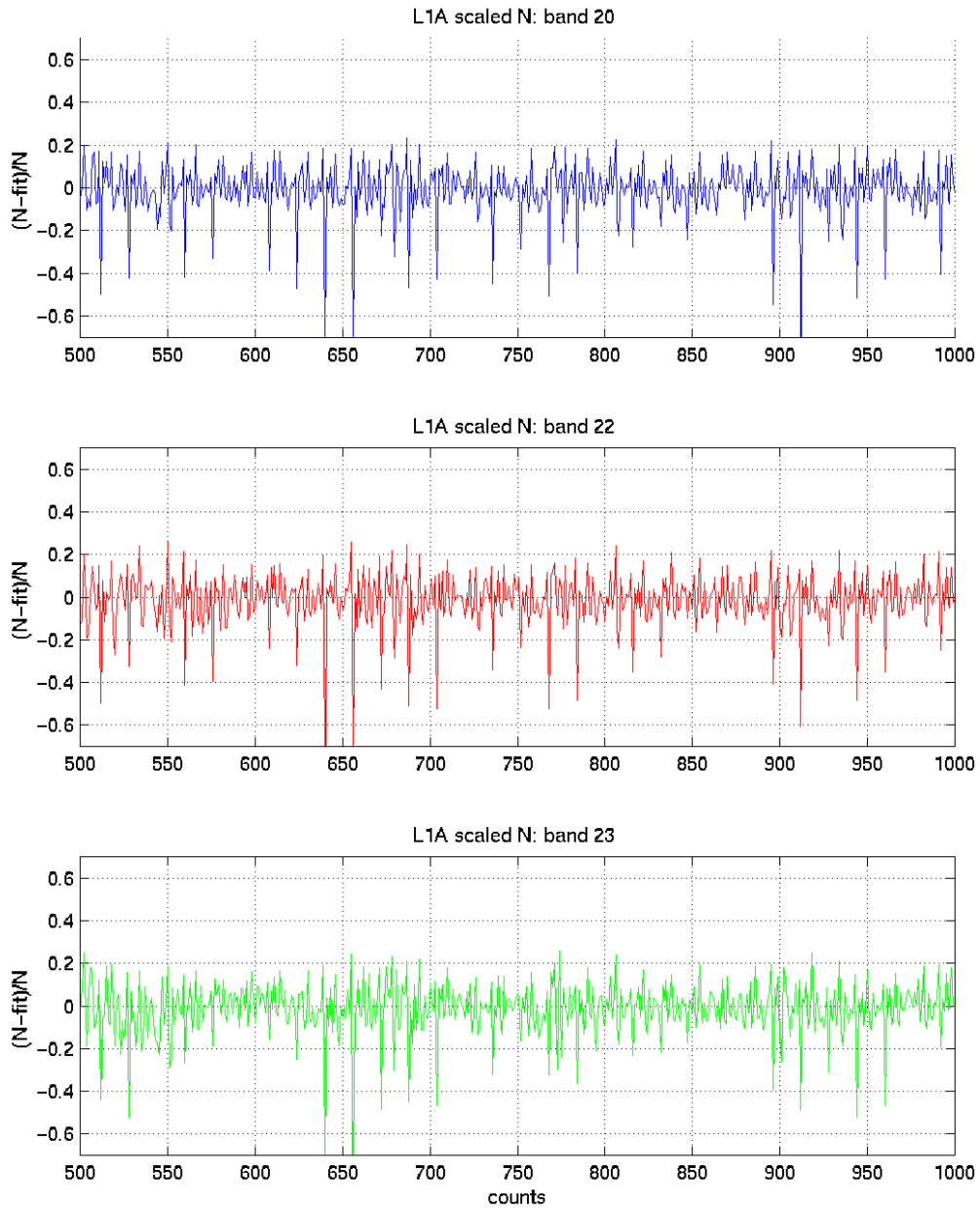


Figure 2. Histogram of the occurrence of digital counts in Bands 20, 22 and 23 at Level 1a processing for one granule, referenced to a polynomial fit. This shows the repeating patterns of anomalous distributions of counts. Only part of the distribution is shown.

MOD01SS.A2000092.0145.001.2000093084628.hdf

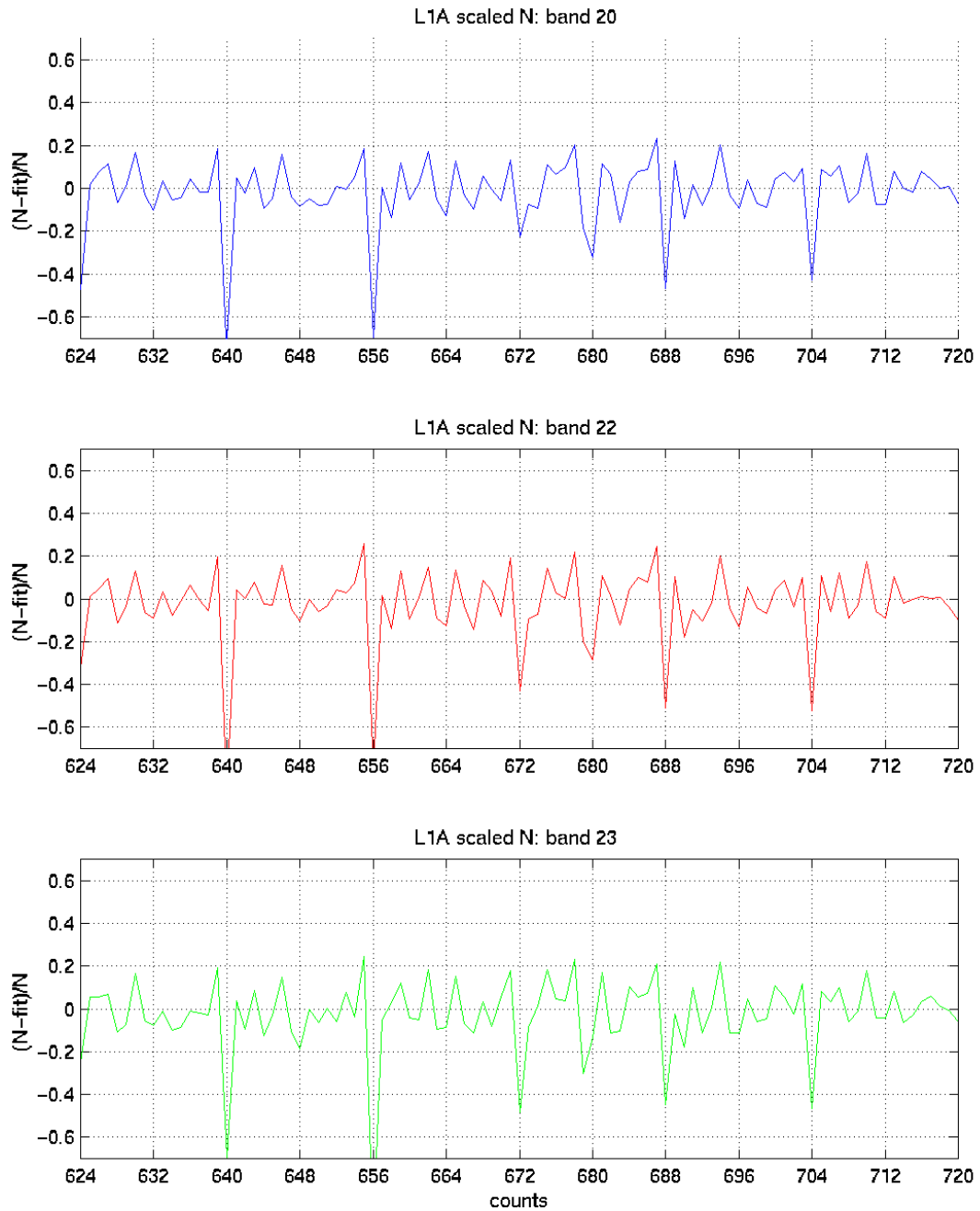


Figure 3. As Figure 2, but on an expanded horizontal scale.

MOD01SS.A2000092.0145.001.2000093084628.hdf  
L1A N: bands 20 (blue), 22 (red), and 23 (green)

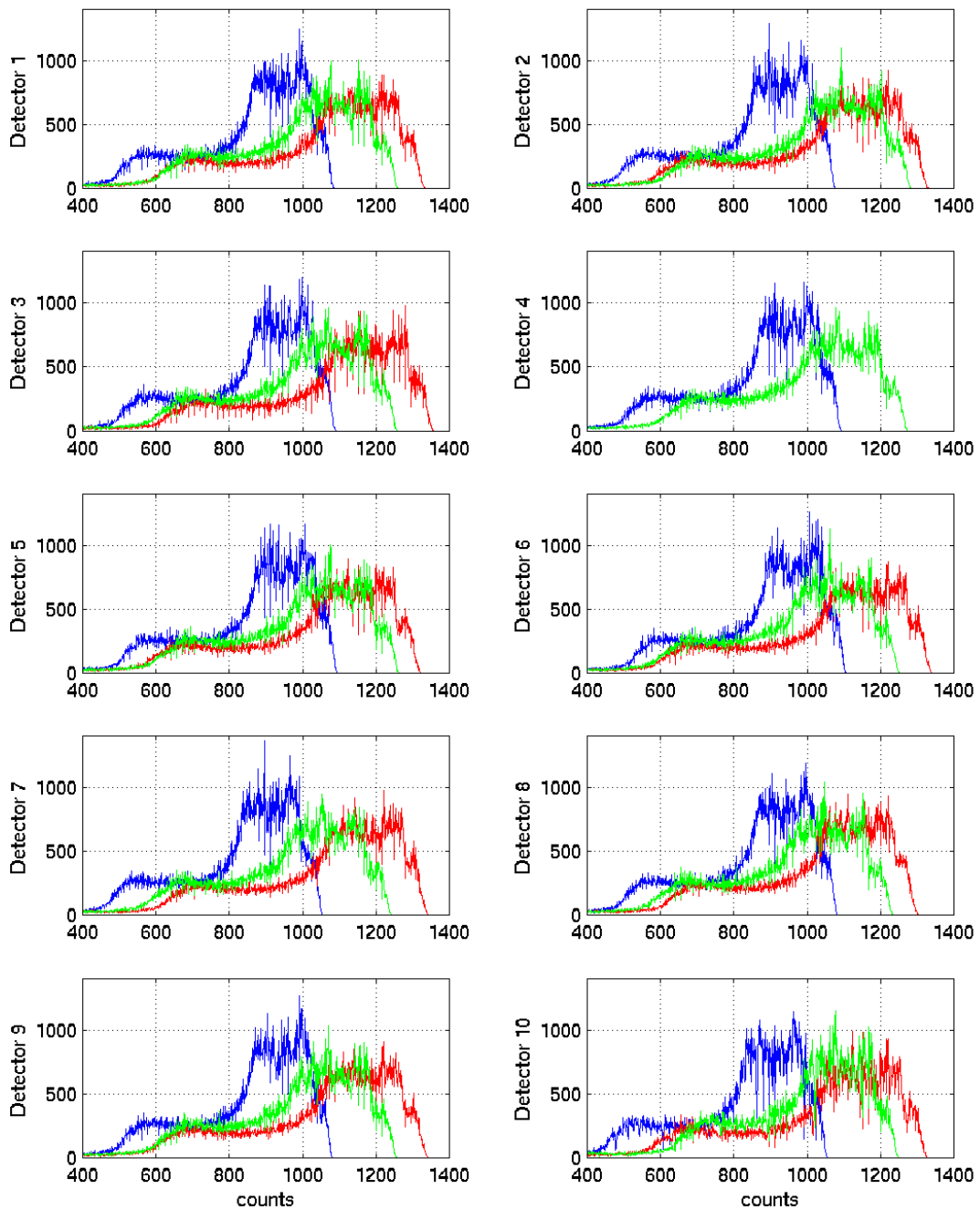


Figure 4. As figure 1, but output from each channel (detector) shown separately. Note the output from detector 4 of band 22 is biased off-scale.

MOD01SS.A2000092.0145.001.2000093084628.hdf

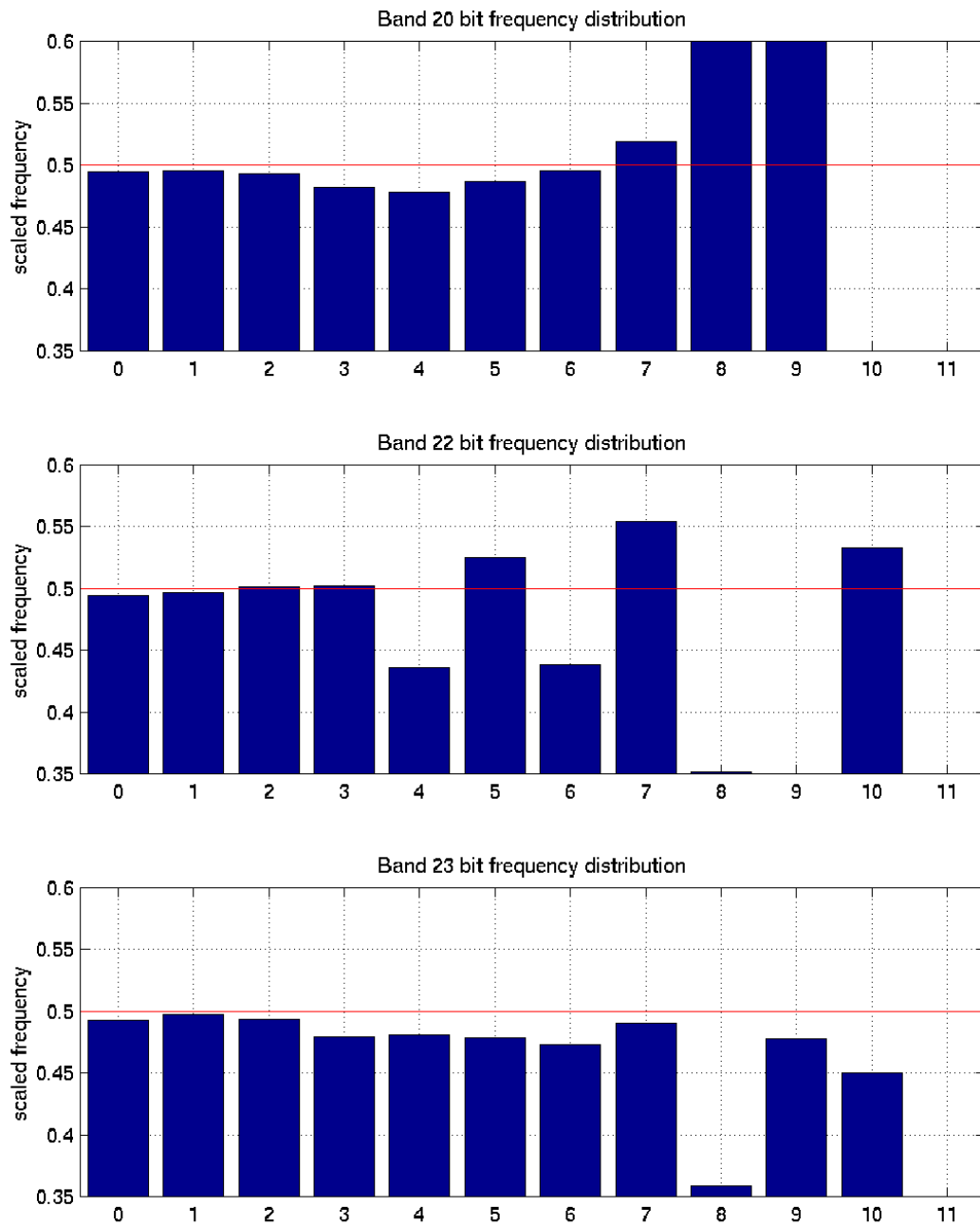


Figure 5. Histograms of bit occupancy for the data, the histogram of which is shown in Figure 1.

MOD01SS.A2000092.0145.001.2000093084628.hdf  
 Band 20 bit frequency distribution

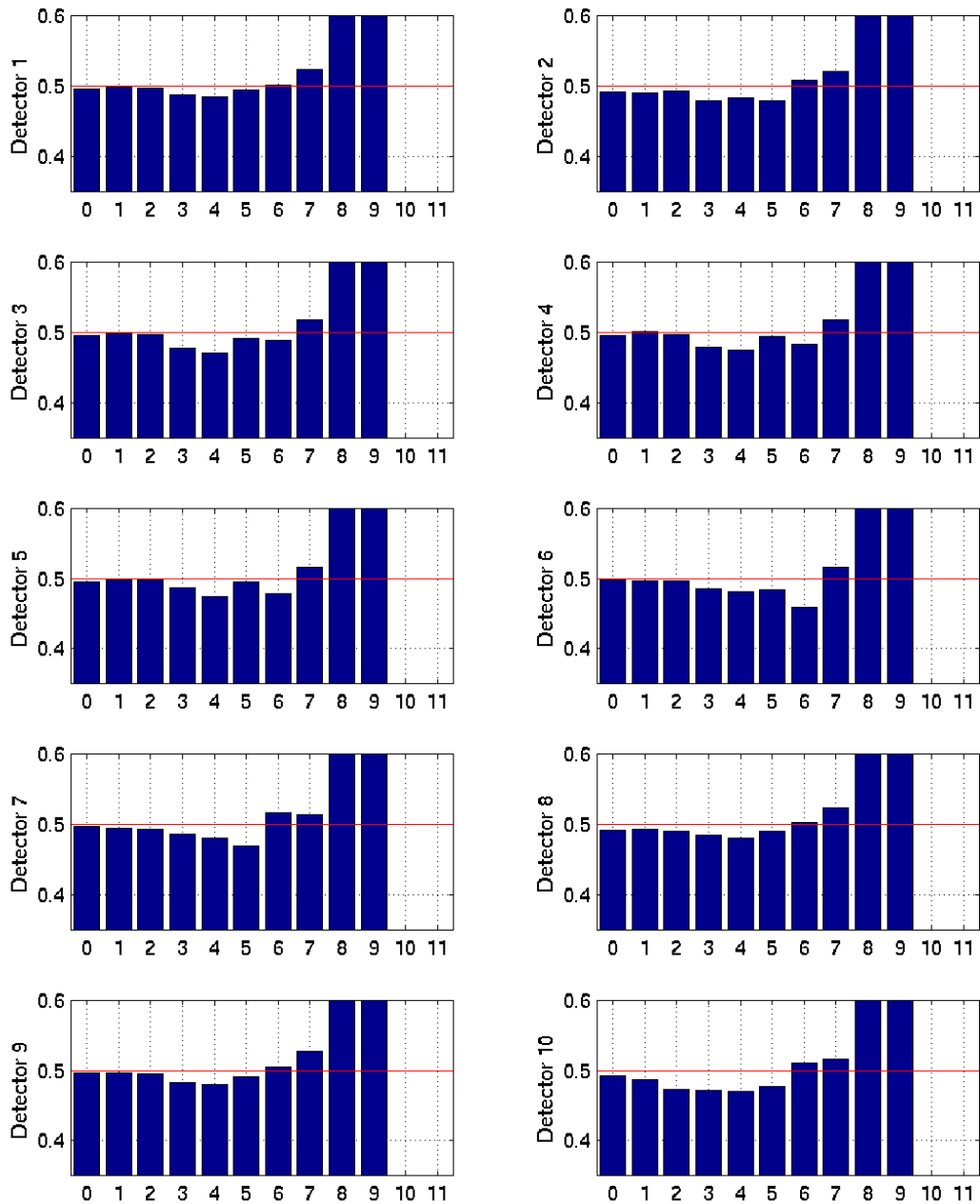


Figure 6. Histograms of bit occupancy for the individual channels (detectors) for band 20 for the granule of data, the histogram of which is shown in Figures 1 and 4.

MOD01SS.A2000092.0145.001.2000093084628.hdf  
 Band 22 bit frequency distribution

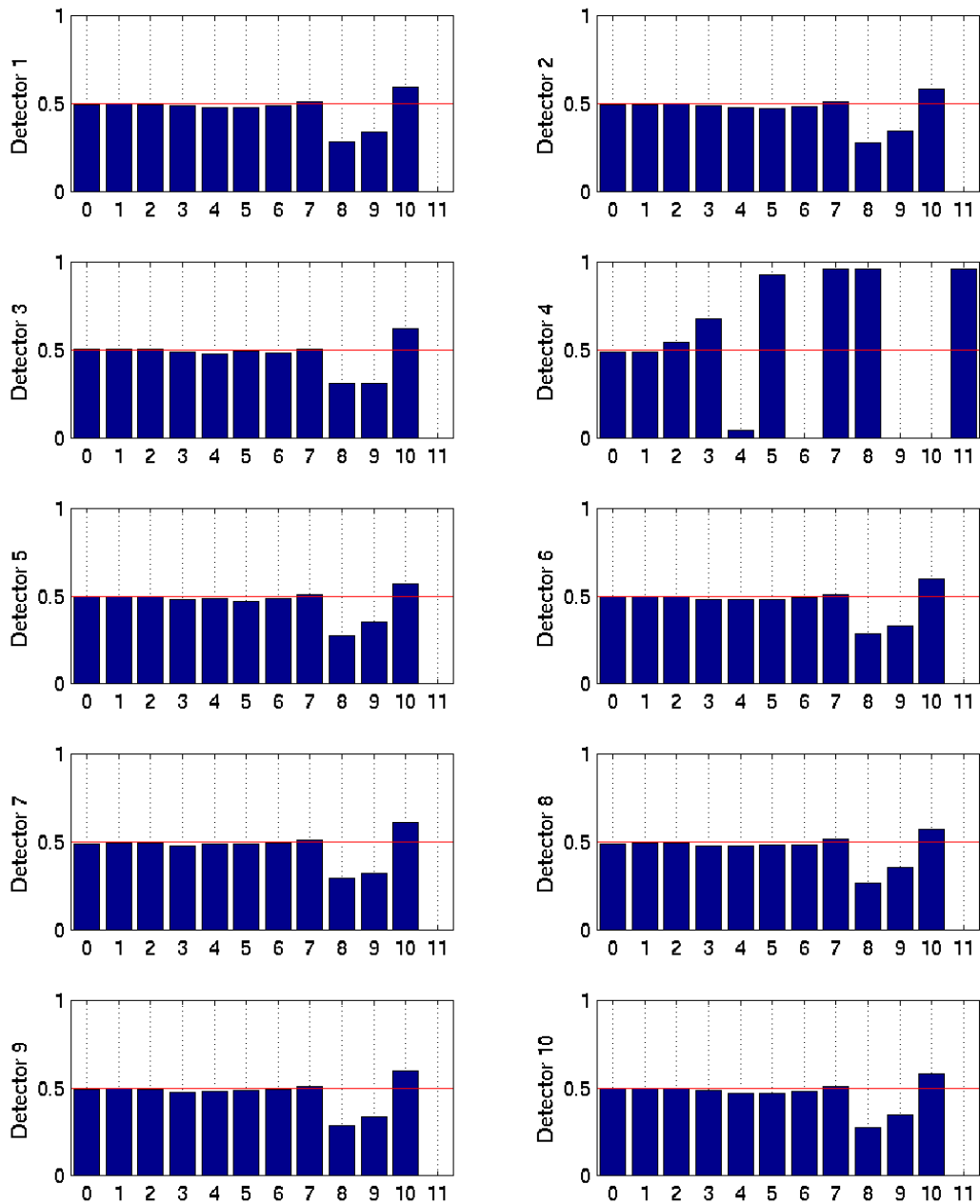


Figure 7. Histograms of bit occupancy for the individual channels (detectors) for band 22 for the granule of data, the histogram of which is shown in Figures 1 and 4. Note that the output from detector 4 is biased off-scale.

MOD01SS.A2000092.0145.001.2000093084628.hdf  
 Band 23 bit frequency distribution

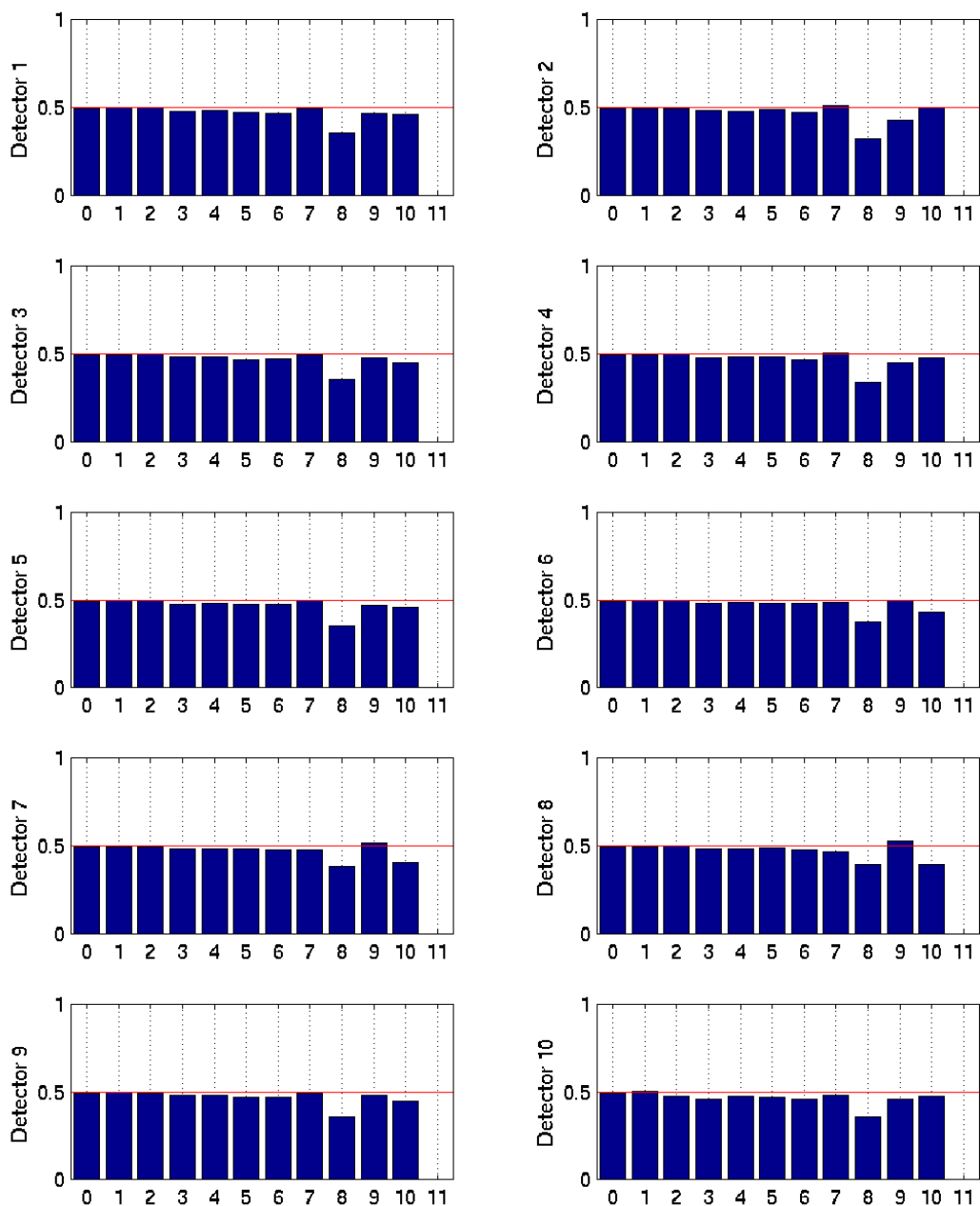


Figure 8. Histograms of bit occupancy for the individual channels (detectors) for band 23 for the granule of data, the histogram of which is shown in Figures 1 and 4.

Band 20 day 90 : #granules=15 #pixels (per detector) =4284000

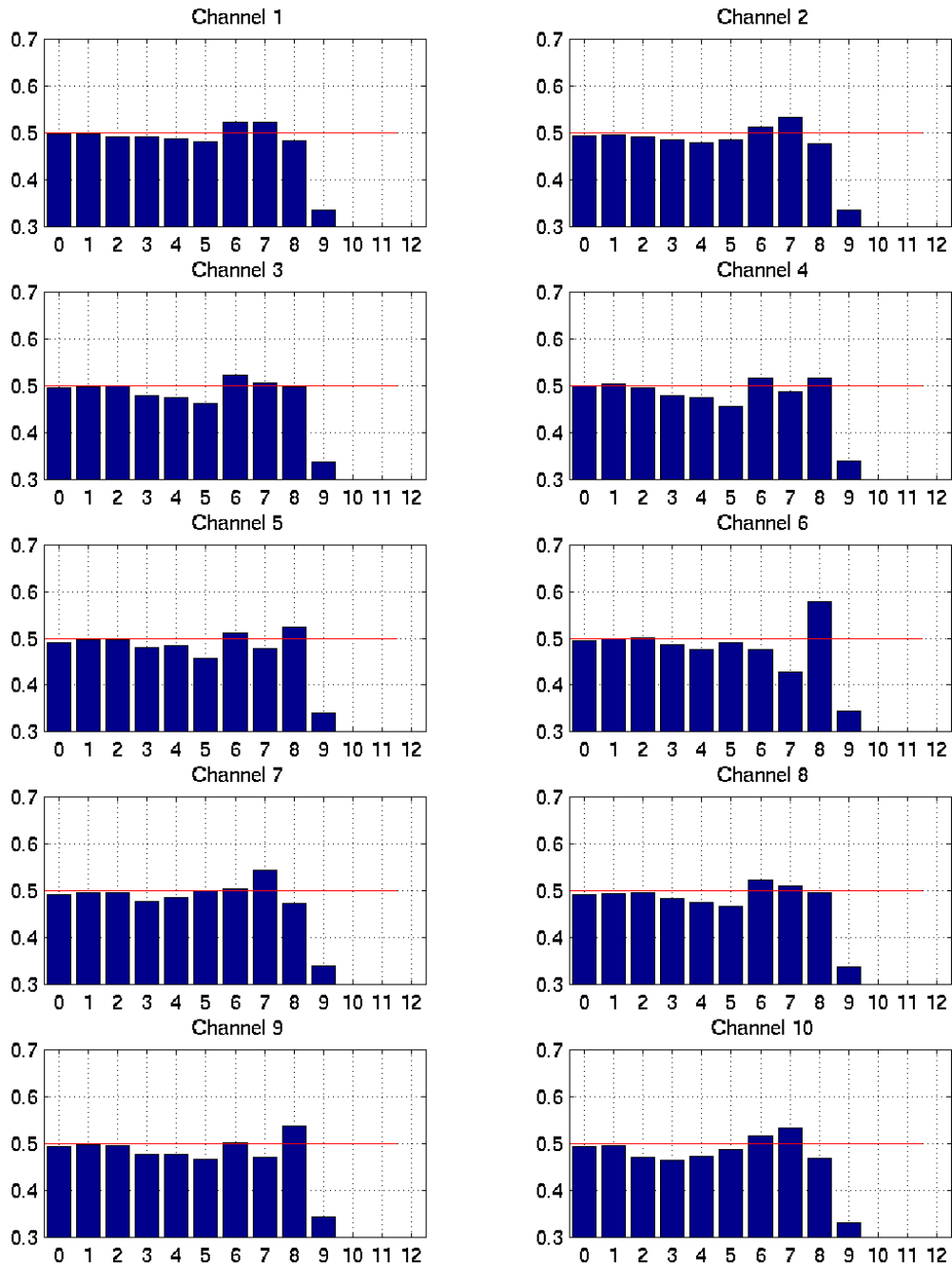


Figure 9. Histograms of bit occupancy for the individual channels (detectors) for band 20 for 15 granules of data.

Band 22 day 90 : #granules=15 #pixels (per detector) =4284000

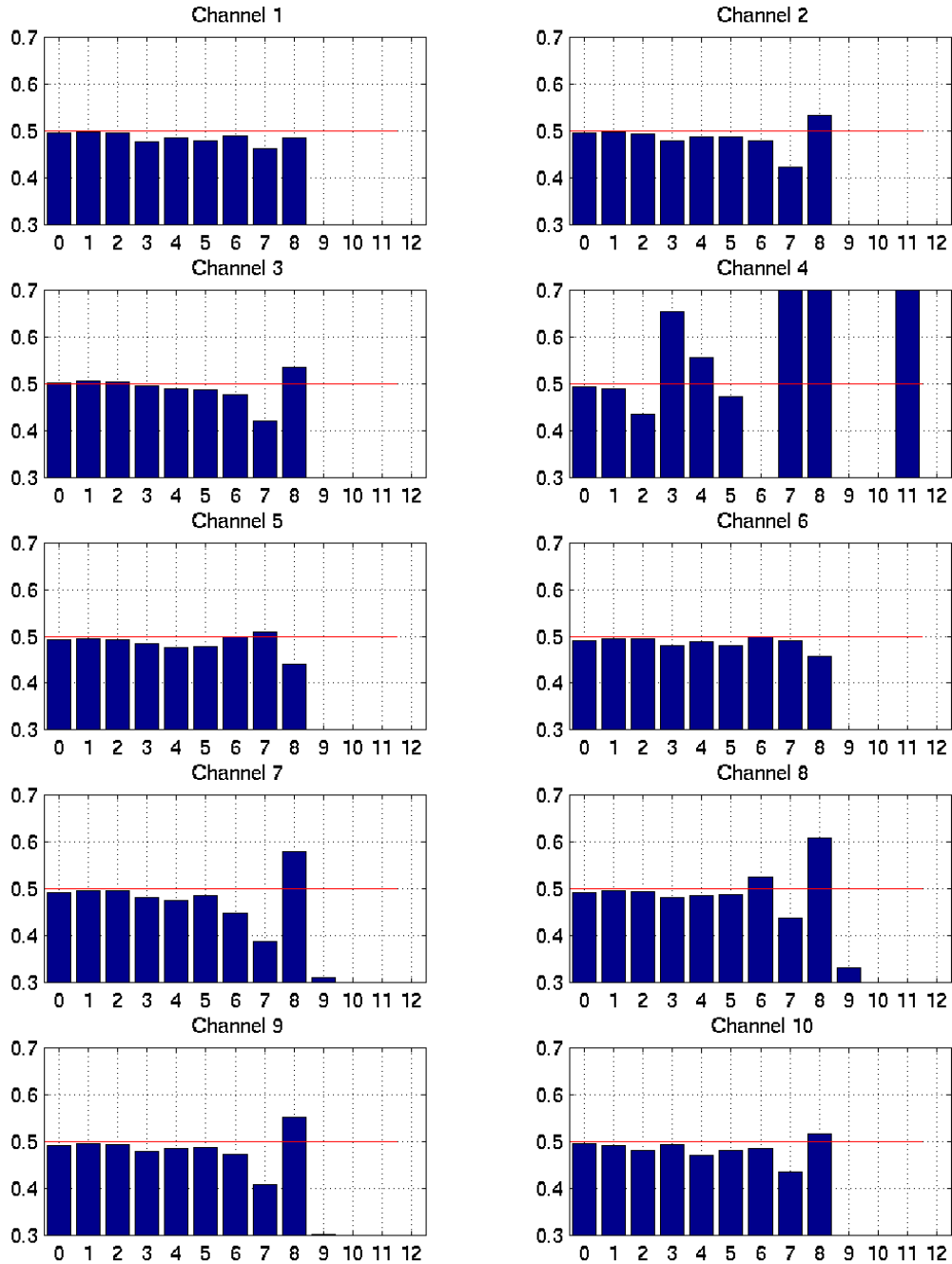


Figure 10. Histograms of bit occupancy for the individual channels (detectors) for band 22 for 15 granules of data. Note that the output from detector 4 is biased off-scale.

Band 23 day 90 : #granules=15 #pixels (per detector) =4284000

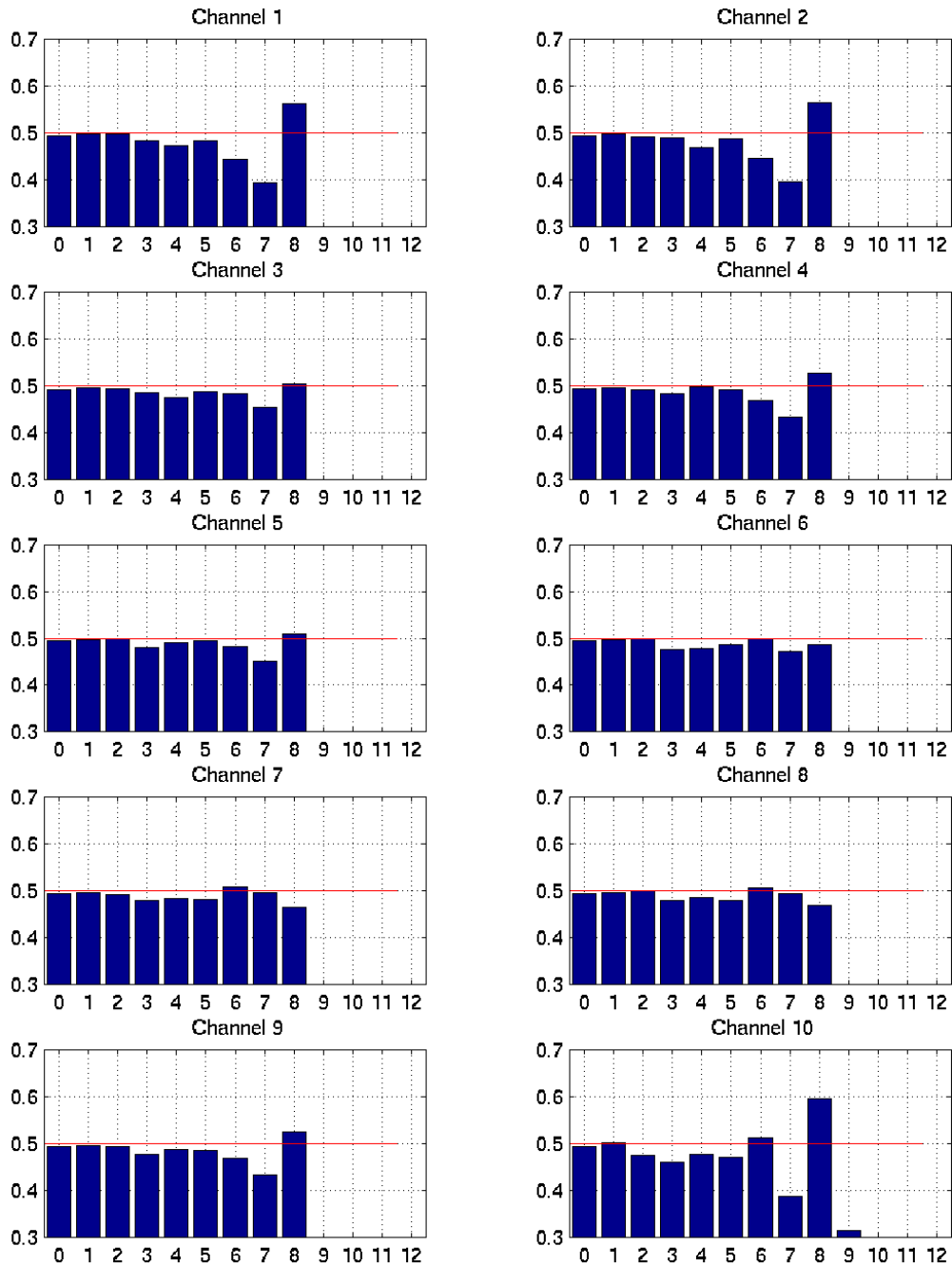


Figure 11. Histograms of bit occupancy for the individual channels (detectors) for band 23 for 15 granules of data.

MOD01SS.A2000092.0145.001.2000093084628.hdf

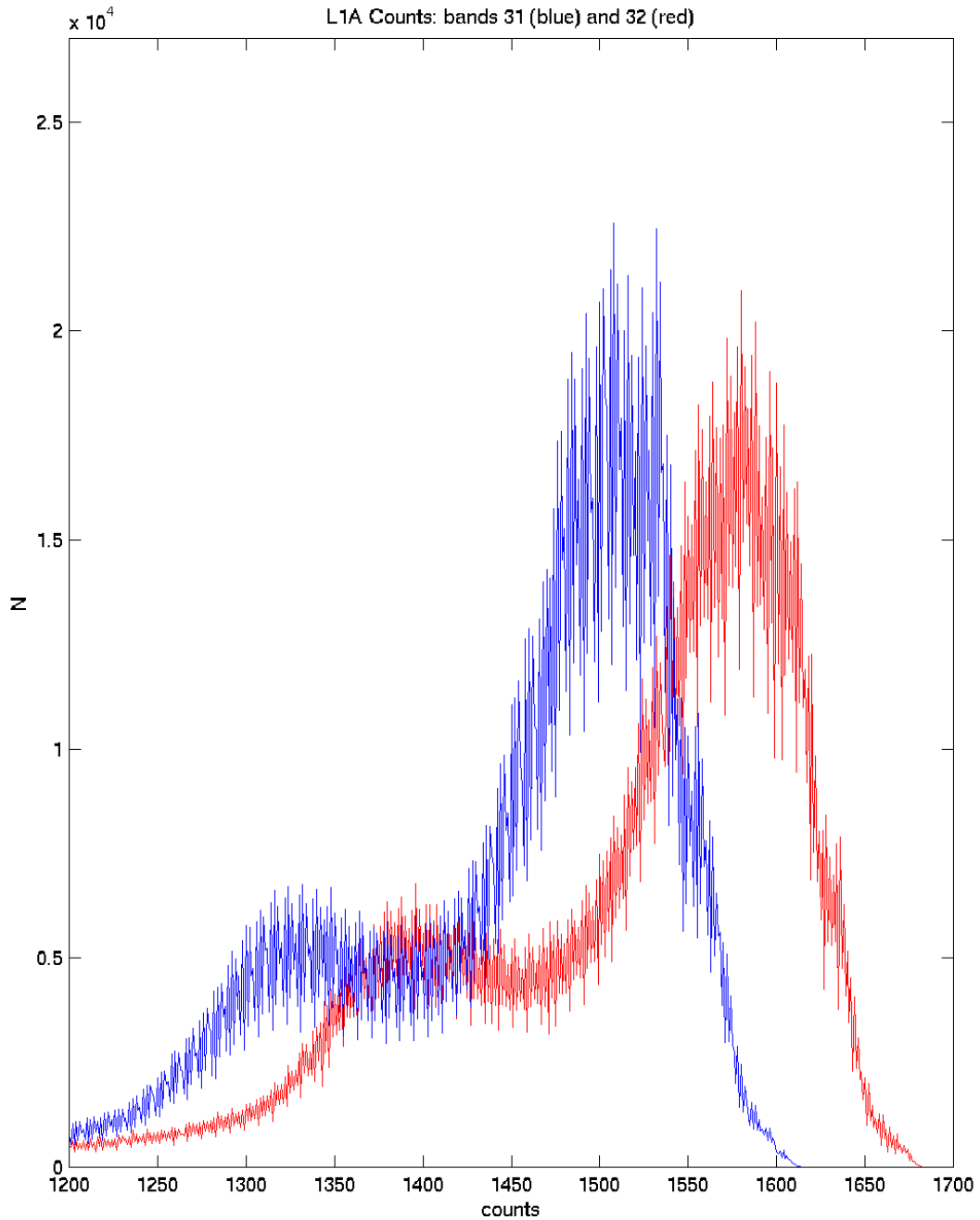


Figure 12. Histogram of the occurrence of digital counts in Bands 31 and 32 at Level 1a processing for one granule. Output from all channels (detectors) are shown.

MOD01SS.A2000092.0145.001.2000093084628.hdf

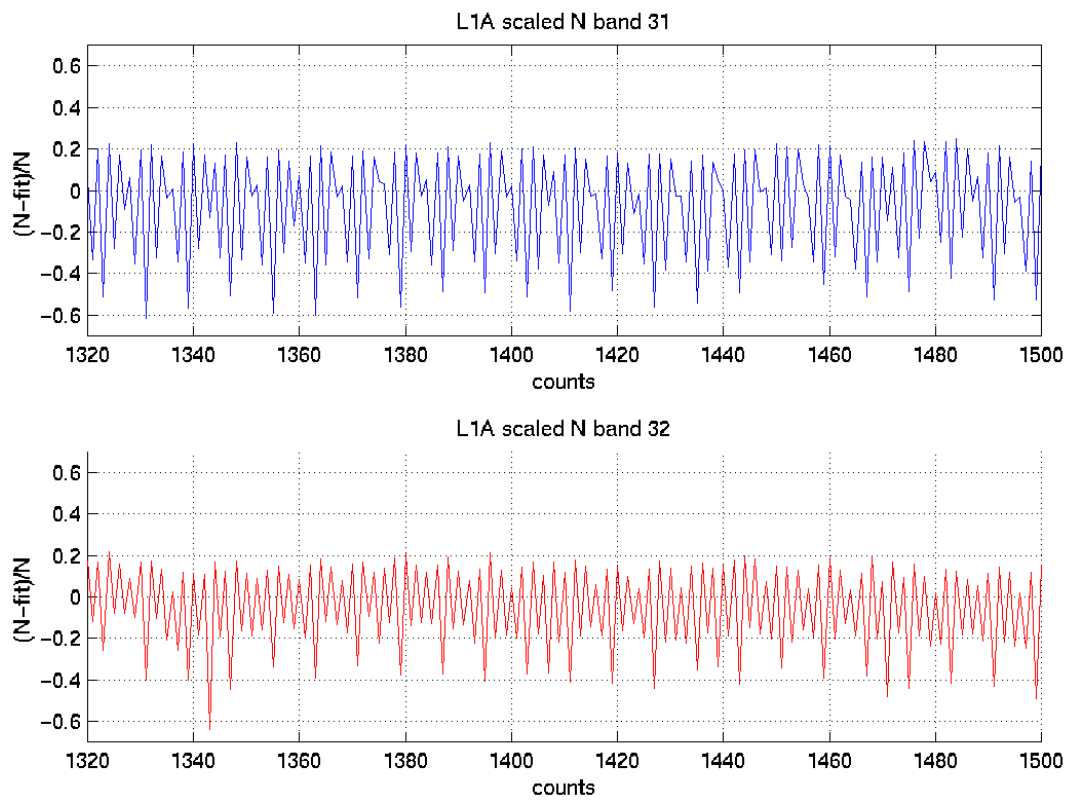


Figure 13. Histogram of the occurrence of digital counts in Bands 31 and 32 at Level 1a processing for one granule, referenced to a polynomial fit. This shows the repeating patterns of anomalous distributions of counts. Only part of the distribution is shown.

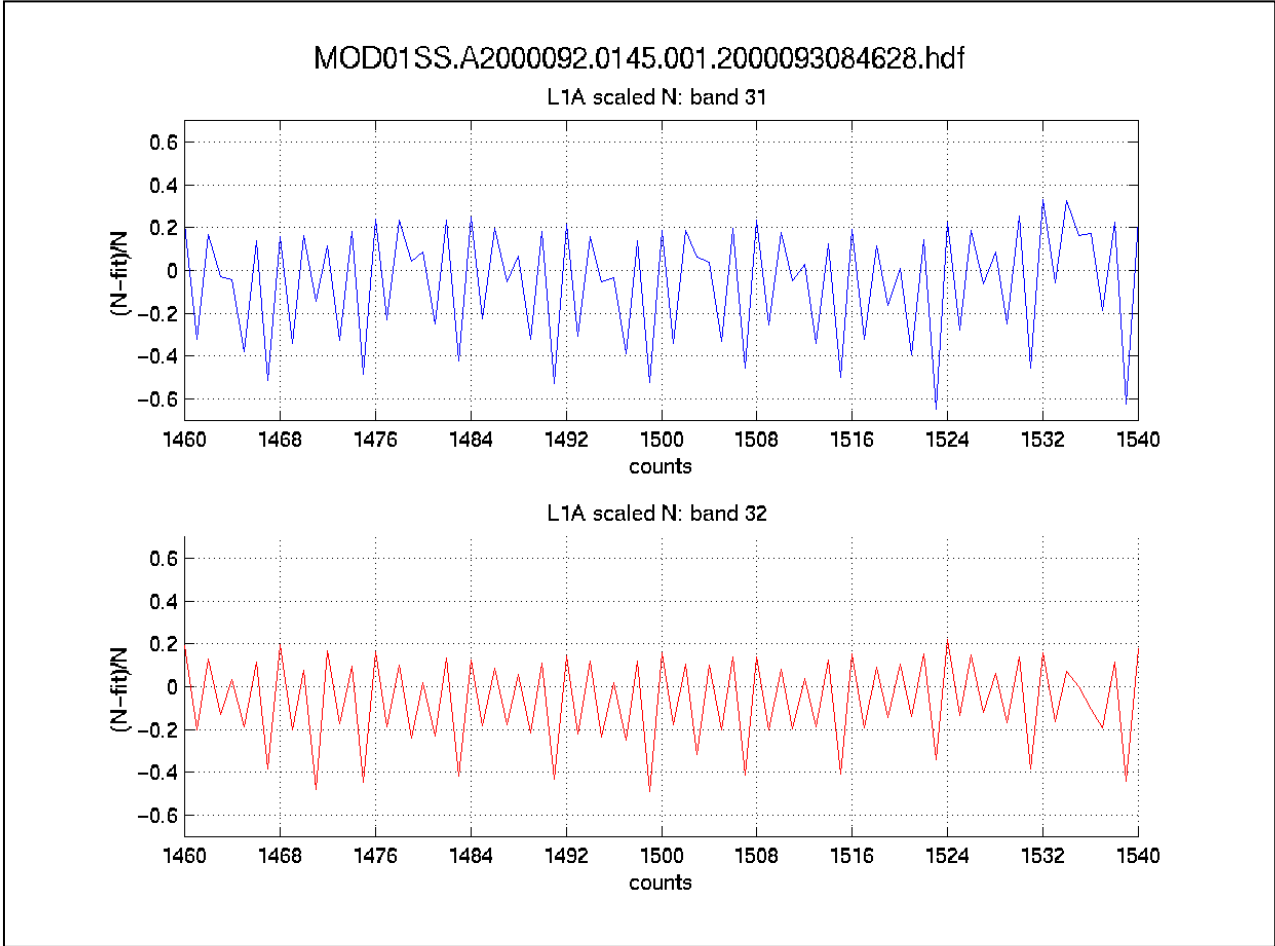


Figure 14. As Figure 13, but on an expanded horizontal scale.

MOD01SS.A2000092.0145.001.2000093084628.hdf  
L1A N : bands 31 (blue) and 32 (red)

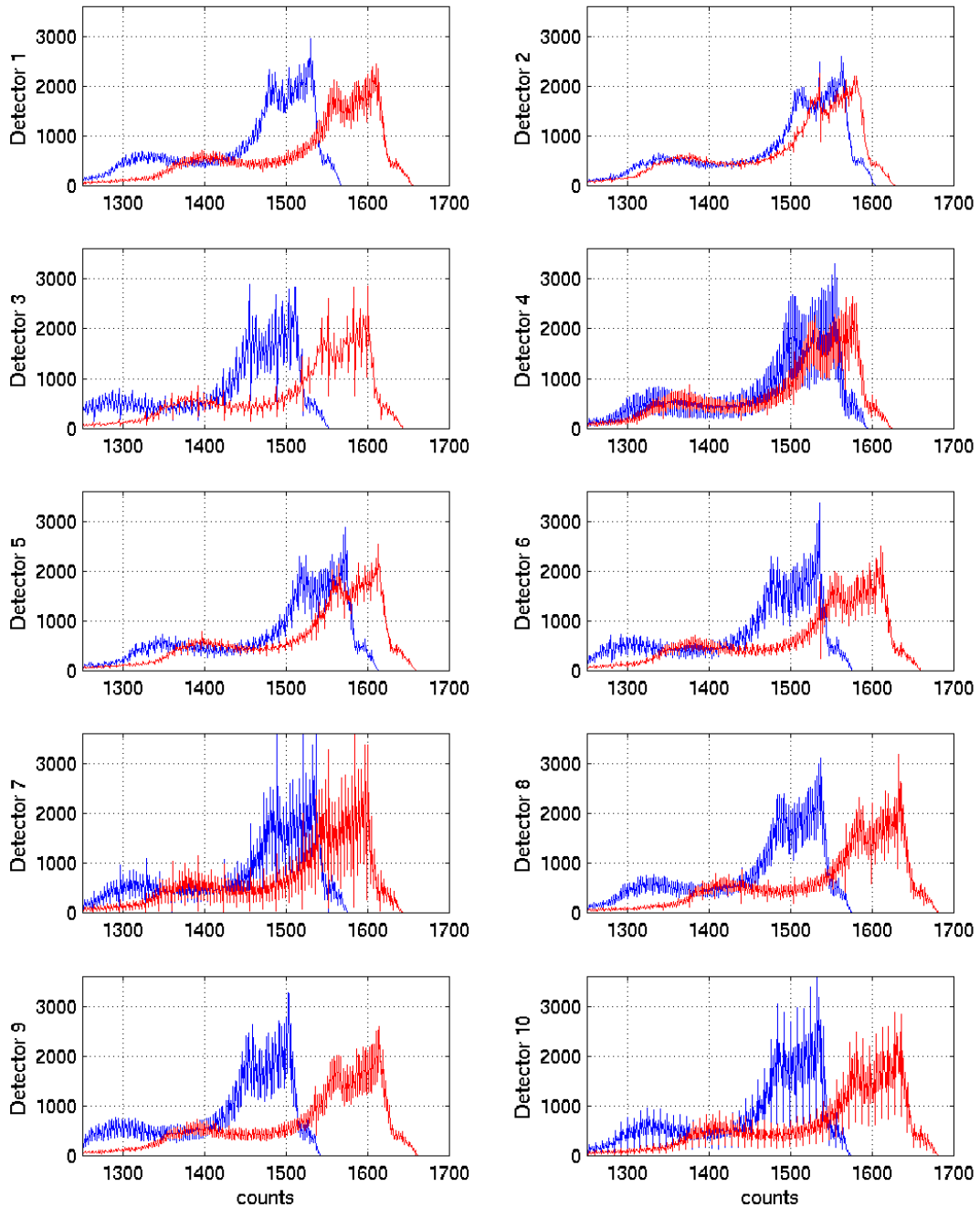


Figure 15. As figure 12, but output from each channel (detector) shown separately.

MOD01SS.A2000092.0145.001.2000093084628.hdf  
 Band 31 bit frequency distribution

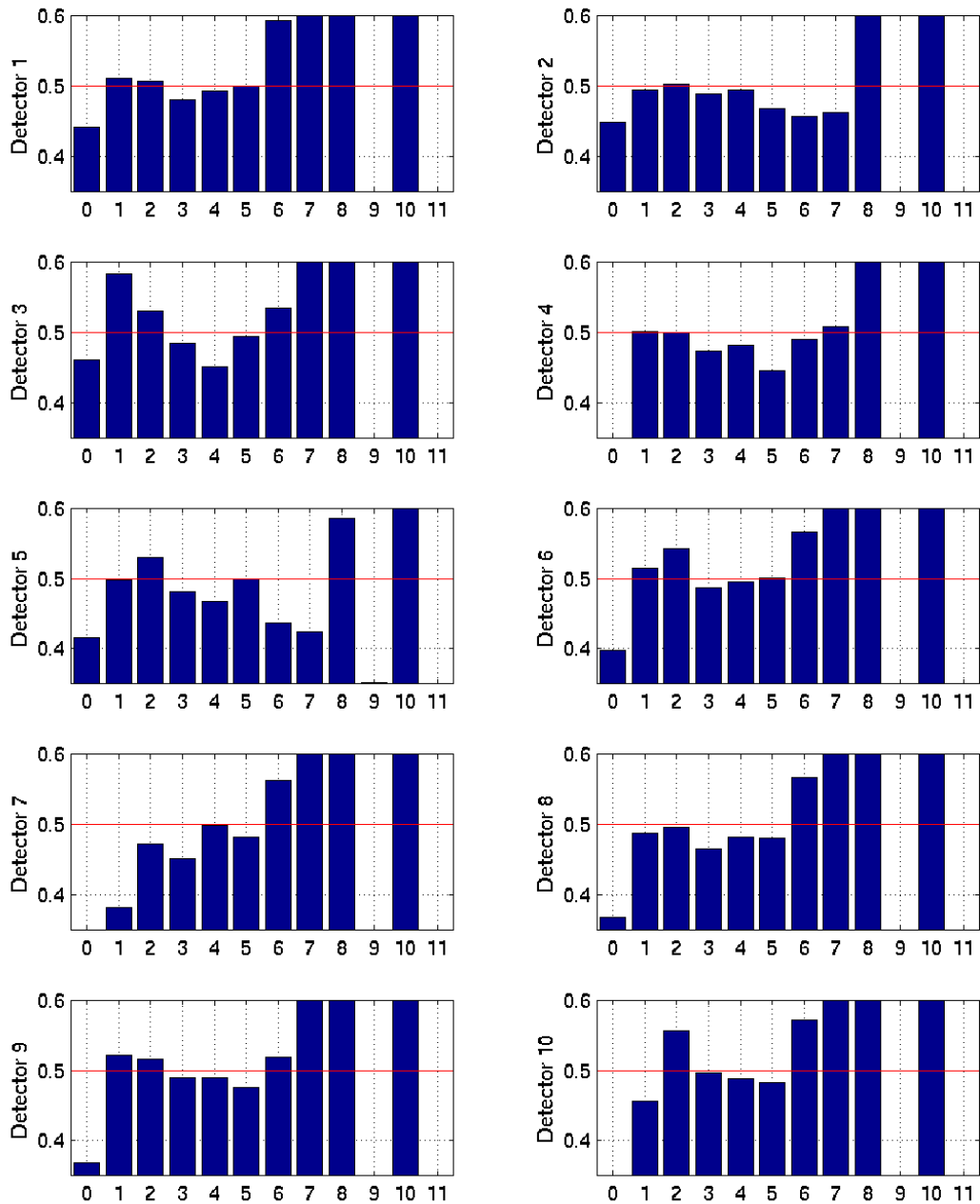


Figure 16. Histograms of bit occupancy for the individual channels (detectors) for band 31 for the granule of data, the histogram of which is shown in Figures 12 and 15.

MOD01SS.A2000092.0145.001.2000093084628.hdf  
 Band 32 bit frequency distribution

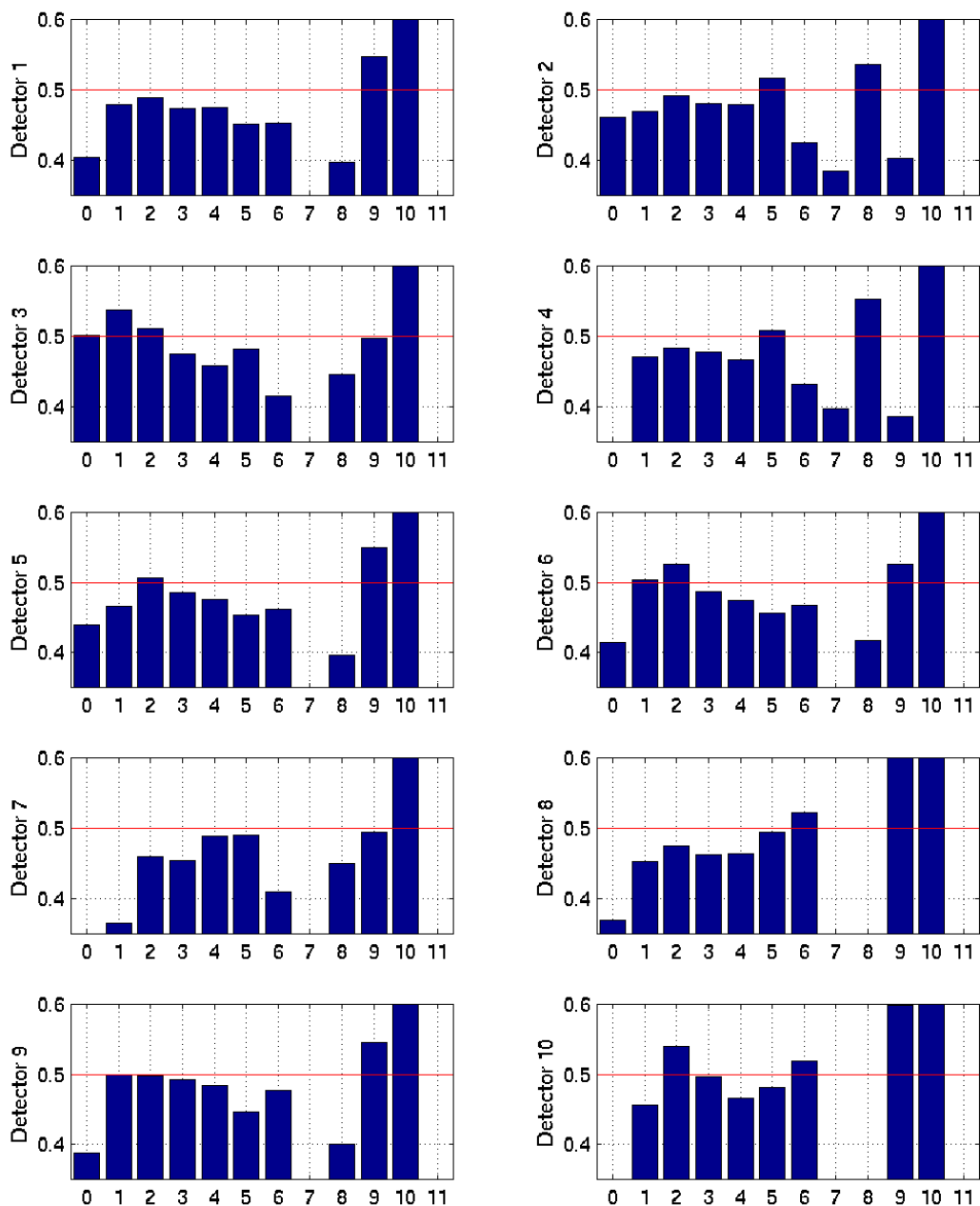


Figure 17. Histograms of bit occupancy for the individual channels (detectors) for band 32 for the granule of data, the histogram of which is shown in Figures 12 and 15.

Band 31 day 90 : #granules=15 #pixels (per detector) =4284000

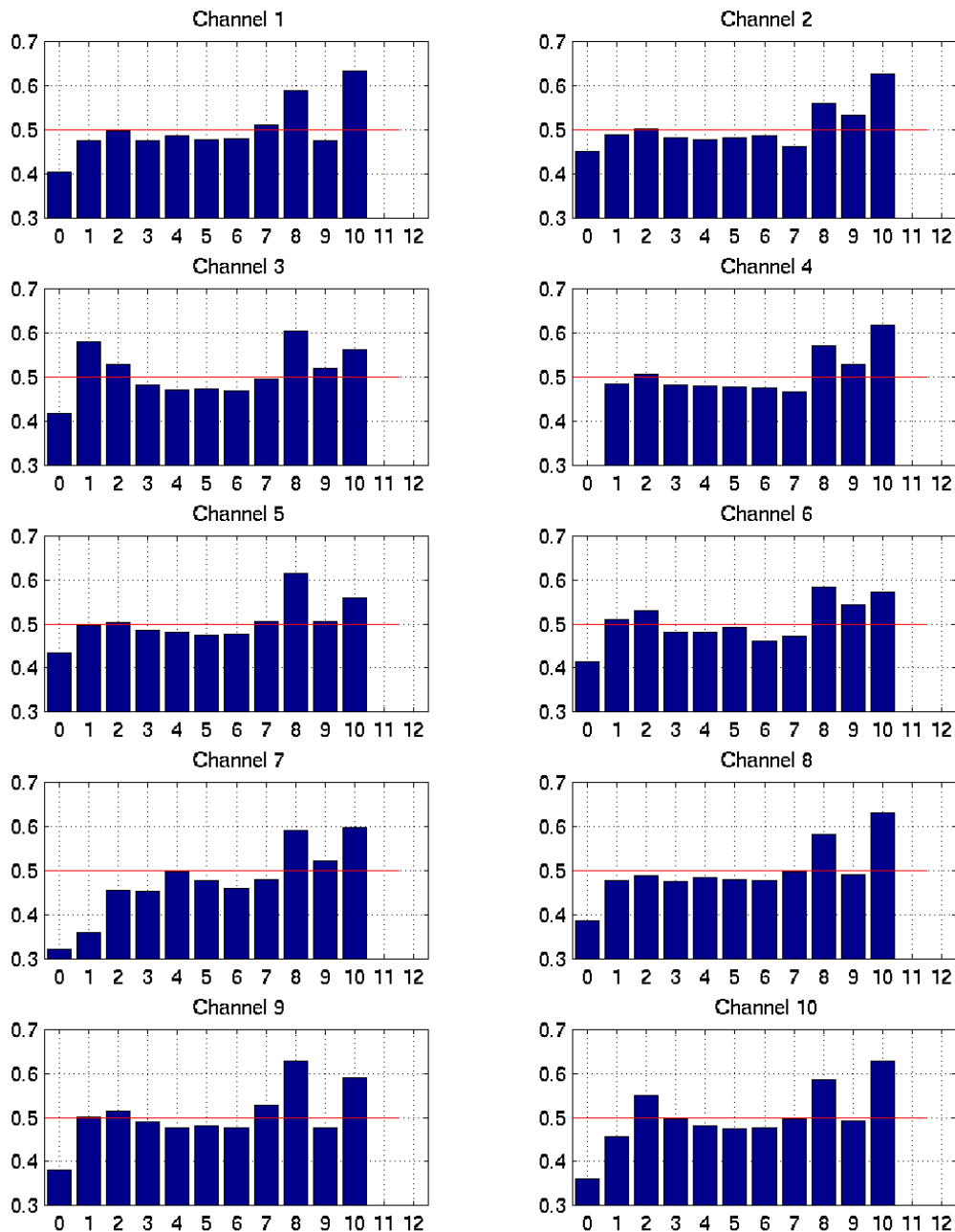


Figure 18. Histograms of bit occupancy for the individual channels (detectors) for band 31 for 15 granules of data.

Band 32 day 90 : #granules=15 #pixels (per detector) =4284000

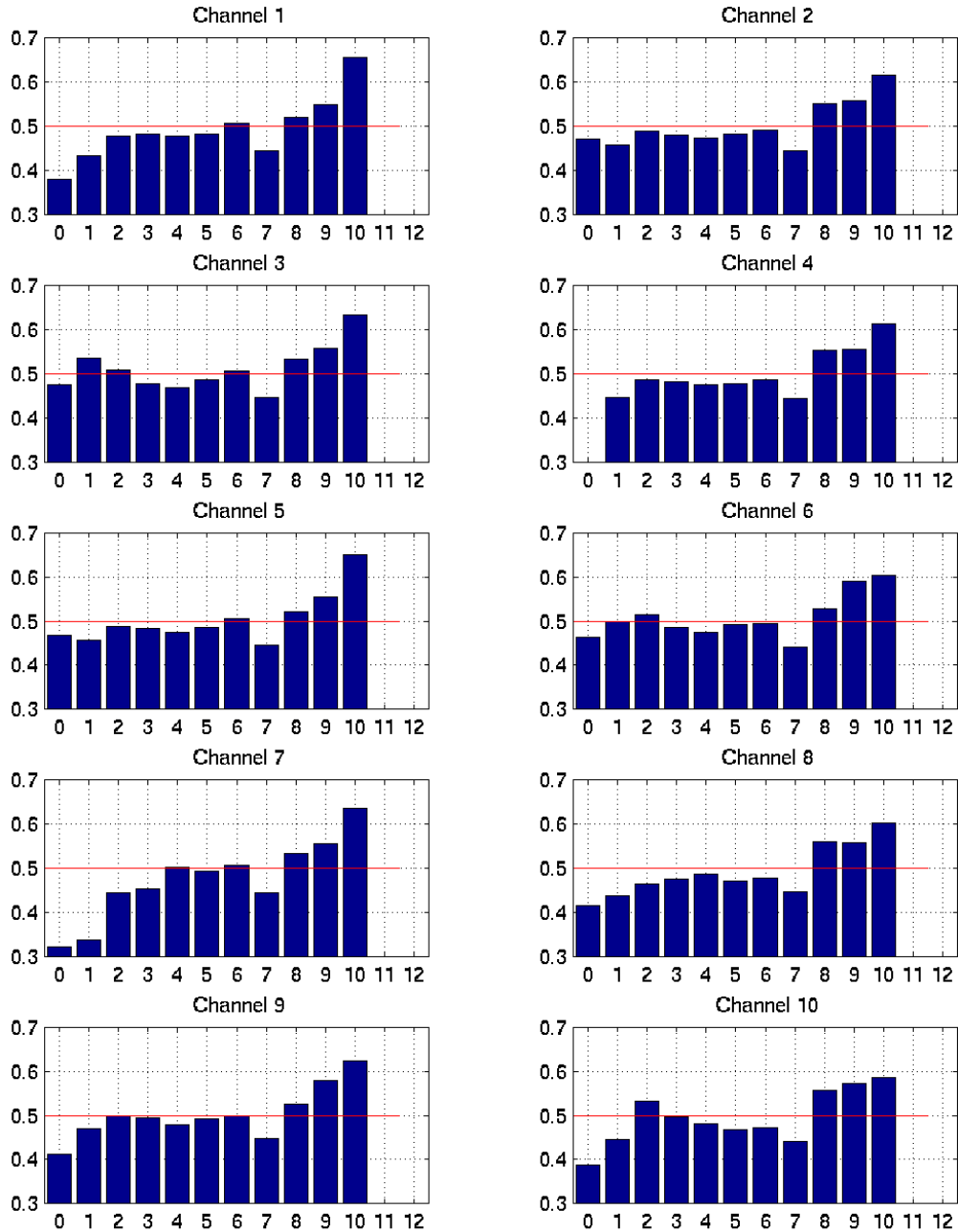


Figure 19. Histograms of bit occupancy for the individual channels (detectors) for band 32 for 15 granules of data.